CORA Cork Open Research Archive
Cartlann Taighde Oscailte Chorcaí

Title	Ferroelectric nanoparticles, wires and tubes: synthesis, characterisation and applications
Authors	Varghese, Justin M.;Whatmore, Roger W.;Holmes, Justin D.
Publication date	2013-02-11
Original Citation	VARGHESE, J., WHATMORE, R. W. & HOLMES, J. D. 2013. Ferroelectric nanoparticles, wires and tubes: synthesis, characterisation and applications. Journal of Materials Chemistry C, 1, 2618-2638. http://dx.doi.org/10.1039/C3TC00597F
Type of publication	Article (peer-reviewed)
Link to publisher's version	http://pubs.rsc.org/en/content/articlepdf/2013/tc/c3tc00597f - 10.1039/C3TC00597F
Rights	© Royal Society of Chemistry 2013.
Download date	2026-10-29 12:14:51
Item downloaded from	https://hdl.handle.net/10468/2271

UCC
University College Cork, Ireland
Coláiste na hOllscoile Corcaigh

Journal Name

Dynamic Article Links ►

Cite this: DOI: 10.1039/c0xx00000x

www.rsc.org/xxxxxx

FEATURE ARTICLE

Nanoferroelectrics: Fabrication, Characterisation and Applications of Zero and One-Dimensional Materials

Justin Varghese,[a, b, c] Roger W. Whatmore[b] and Justin D. Holmes *[a, b, c]

Received (in XXX, XXX) Xth XXXXXXXXX 20XX, Accepted Xth XXXXXXXXX 20XX
DOI: 10.1039/b000000x

Nanostructured materials are central to the evolution of future electronics and information technologies. Ferroelectrics have already been established as a dominant branch in the electronics sector because of their diverse application range such as ferroelectric memories, ferroelectric tunnel junctions, etc. The on-going dimensional downscaling of materials to allow packing of increased numbers of components onto integrated circuits provides the momentum for the evolution of nanostructured ferroelectric materials and devices. Nanoscaling of ferroelectric materials can result in a modification of their functionality, such as phase transition temperature or Curie temperature (T_C), domain dynamics, dielectric constant, coercive field, spontaneous polarisation and piezoelectric response. Furthermore, nanoscaling can be used to form high density arrays of monodomain ferroelectric nanostructures, which is desirable for the miniaturisation of memory devices. This review article highlights some exemplary research breakthroughs in the fabrication, characterisation and applications of zero and one-dimensional nanoscale ferroelectric materials over the last decade, with priority given to novel synthetic strategies.

1. A Short History of Ferroelectricity and Piezo-electricity

In 1880 brothers Pierre and Paul-Jacques Curie discovered the existence of piezoelectricity in various crystals like quartz, tourmaline and Rochelle salt.[1, 2] This discovery provided the drive for further study in the field of piezoelectrics, notably works done by Walter Cady and Erwin Schrödinger.[3, 4] In 1912, Erwin Schrödinger first coined the term "*ferroelektrisch*" or '*ferroelectricity*'.[4] Credit for discovering ferroelectricity goes to Joseph Valasek for his systematic study of the magnetic properties of ferromagnetics and the dielectric properties of Rochelle salt, which he presented at the annual meeting of the American Physical Society in Washington on 23rd April 1920.[5, 6] Another major breakthrough in ferroelectric research happened in the early 1940s, during World War II, with the discovery of ferroelectricity in barium titanate ($BaTiO_3$) and other perovskite-based materials.[7-9] The discovery of ferroelectricity in $BaTiO_3$ opened up new vistas of application for ferroelectric materials, leading to significant interest in other types of ferroelectrics.[10, 11] Since the discovery of ferroelectricity in Rochelle salt 92 years ago, there have been many theoretical and experimental advances in the research area.[11-21] In particular, the last two decades witnessed significant progress in the miniaturisation of electronics components, which resulted in the rapid development of nanoferroelectric research.[12-21]

1.1 A Primer on ferroelectric materials

All materials undergo a small change in their dimensions when subjected to an external force, such as a mechanical stress, an electric field, or even a change in temperature.[10, 22] Depending on the crystal structure of the material, a small dimensional modification by an electric field, a change in temperature or a mechanical stress can create an electric polarisation change inside the crystal and hence give rise to the occurrence of pyroelectricity and piezoelectricity respectively.[10, 22] A material's crystal structure must lack a centre-of-symmetry (be "acentric") for it to show piezoelectricity, and be both acentric and possess a unique axis of symmetry (making it a "polar" structure) for it to be pyroelectric. There are 32 crystal classes, and 11 of them possess a centre of symmetry. Of the remaining 21 acentric classes, all except one exhibit a polarisation change when subjected to mechanical stress and hence are *piezoelectric*.[10, 22] Ten of these 20 classes possess a unique axis of symmetry (are polar) and an electric polarisation exists within the structure in the absence of an applied field. The electric polarisation in these polar materials[10, 22] changes with temperature, making them *pyroelectric*. As they are acentric, they also show piezoelectric behaviour. *Ferroelectrics* are a subgroup of pyroelectrics, in which spontaneous polarisation within the structure can be switched between different stable directions by an application of

an electric field of sufficient magnitude (the coercive field).[10, 22] Figure 1 depicts the basis of piezoelectricity, pyroelectricity and ferroelectricity.

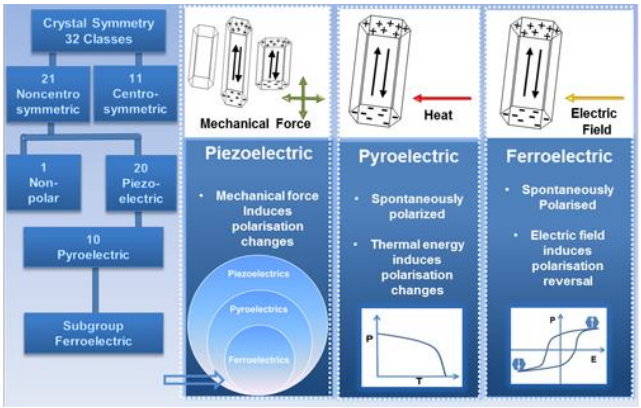

Figure 1. Schematic representation of piezoelectricity, pyroelectricity and ferroelectricity on the basis of crystal symmetry (Column 1) and their origin based on the mode of polarisation change occurring inside the material (Column 2-4). Venn diagram in column 2 shows that all ferroelectric materials are pyroelectric and piezoelectric but not vice versa. The graphs in columns 3 and 4 represent the polarisation (*P*) change with respect to temperature (*T*) and electric field (*E*) respectively.

According to the Landolt–Börnstein data base,[23] ferroelectric materials are classified into three major groups comprising of 72 families; according to their chemical composition and crystal structure.[9] These three ferroelectrics groups are (1) inorganic oxides, (2) inorganic non-oxides, and (3) organic crystals, liquid crystals and polymers.[9, 23] Among these three groups, the oxide-based ferroelectrics especially the ABO_3 perovskite-type family, are the most extensively studied. Commonly studied ferroelectrics such as barium titanate ($BaTiO_3$), lead titanate ($PbTiO_3$) and lead zirconate titanate ($PbZr_xTi_{(1-x)}O_3$) belong to perovskite family.[9, 11, 22] Within the non-oxide ferroelectrics, some chalcogenide and chalcohalide-based materials show promising ferroelectric characteristics, *e.g.* zinc cadmium telluride (ZnCdTe)[24] and antimony sulfoiodide (SbSI)[25]. Within the polymer family, polyvinylidene fluoride (PVDF) and its copolymers with trifluoroethylene show excellent ferroelectric and piezoelectric characteristics.[26] A more detailed description of different types of ferroelectric families can be found elsewhere.[9, 23]

1.2 Nanoscale Ferroelectrics and Piezoelectrics

Materials in the nanostructured form are central to the evolution of future electronics and information technologies. Ferroelectrics have already been established as a dominant branch in the electronics sector, because of their diverse application range. The on-going dimensional downscaling of materials, to cram more components onto integrated circuits, in turn gives a great boost to the evolution of potential nanostructured ferroelectric materials and devices.[12-21] For instance, memory storage based on ferroelectric polarisation reversal has been predicted as one of the emerging memory technologies[12], owing to their high read-write speed, low power consumption and long rewriting endurance.[27, 28]

Size and dimensionality plays a critical role in determining the ferroelectric characteristics of a material at the nanoscale, due to the different ways in which dipoles align in ferroelectric crystals. Since ferroelectricity is a cooperative phenomenon caused by the arrangement of charge dipoles within a crystal structure, an increase in surface area by nanostructuring could trigger immense changes in the long- and short-range ordering of dipoles inside a material. These changes could alter some of the ferroelectric functionality, such as phase transition temperature or Curie temperature (T_C), domain dynamics, dielectric constant, coercive field, or spontaneous polarisation, piezoelectric response, *etc*., at the nanoscale.[14, 21, 29-35] In short, low dimensional ferroelectrics show marked deviations in their properties compared to their bulk ferroelectric counterparts, mostly due to the great enhancement of surface area. Since the surface characteristics of nanostructures are morphology and size dependent, the type of nanostructuring used in ferroelectrics must be based on the dependence of some parameter related to the ferroelectric functionality under consideration. This parameter could be crystallinity, alignment, ordering or even surface modification of the ferroelectric nanostructures under consideration.[36]

This review article highlights some breakthroughs that outline the progress in research in nanoscale ferroelectric material syntheses, characterisations and applications (excluding thin films) covering mostly the last decade, with priority given to novel synthetic strategies. The 'bottom-up' and 'top-down' approaches used so far for synthesising nanoscale ferroelectrics of various morphology and structuring will be discussed in detail, whilst highlighting the pros and cons of each synthetic strategy. This review will also address the current efforts in making precisely ordered ferroelectric nanostructures. All of the developments in the synthesis of nanoscale ferroelectrics will not be complete without a proper choice of characterisation tools to study the ferroelectric features at the nanoscale, and these techniques will be also discussed; focusing on scanning probe based techniques, especially piezoresponse microscopy (PFM), as these are the vital characterisation tools to investigate the ferroelectric and piezoelectric functionality at the nanoscale.[37-46] The concluding section will give a summary on emerging nanoferroelectric applications and the future outlook of the entire field of nanoferroelectric research.

1.3 Classification of Ferroelectric Nanostructures

Generally nanostructured materials fall into 4 different classes, *viz*. zero-dimensional (0D; nanoparticles), one-dimensional (1D; nanowires, nanotubes and nanorods), two-dimensional (2D; thin films, nanodot arrays, and lamellae patterns), and three-dimensional (3D; vertically aligned nanowires, rods or tubes) nanostructures.[47] Over the last decade considerable progress in the fabrication of various nanoscale ferroelectric materials, in a number of novel geometries, has been achieved.[15-17, 19, 20, 48-50]

This journal is © The Royal Society of Chemistry [year]

Table 1. Survey of some recent developments in the synthesis of ferroelectric nanostructures.

Family	Compounds	Experimental methods	Nano-morphology
Pervoskite	$BaTiO_3$	Sol-gel,[51, 52] metal-organic decomposition,[53, 54, 55] PLD,[56] hydrothermal,[57-63] supercritical,[64] templated,[51, 65-70] electrophoretic deposition,[71] surfactant-assisted,[72] molten-salt,[73-76] FIB,[77-79] electro-spinning.[52]	rod,[54, 71, 74, 76, 78] wire,[55, 58, 65, 66, 73, 79] belt,[73] tube,[51, 59, 70] cube,[61, 63] particle,[53, 57, 60, 64, 72] lamella,[77] fibre,[52] torus,[62] dot array.[56, 67-69]
	$(Ba,Sr)TiO_3$	Solvothermal,[80, 81] templated,[82] sol-gel.[82]	particle,[80, 81] tube.[82]
	$NaTaO_3$	Chemical reduction[83]	rod[83]
	$PbTiO_3$, PZT	Hydrothermal,[84, 85] PLD,[86] EBL-assisted,[87-90] nanoimprint lithography,[91, 92] self-assembly,[93-98] templated,[65, 70, 86, 88, 99-104] electro-spinning,[105-107] sol-gel,[88, 99, 100] molten-salt,[73, 75, 76] FIB.[108-110]	islands,[93-98] particle,[85] dot,[108] rod,[75, 76] wire,[65, 73, 91, 105-107] tube,[70, 88, 101, 102, 104] ordered-array.[84, 86-90, 92, 99, 100, 103, 109]
	PLZT	Hydrothermal[111]	hollow sphere[111]
	$SrTiO_3$	Hydrothermal,[58, 63] metal-organic decomposition,[54] templated,[51] molten-salt.[73]	cube,[63] rod,[54, 74, 76] tube,[51] wire.[58, 73]
	$K_{0.5}Bi_{0.5}TiO_3$	Hydrothermal,[112] sol-gel.[112]	wire[112]
	$Na_{0.5}Bi_{0.5}TiO_3$	Hydrothermal,[113] sol-gel.[113]	whisker[113]
Layered structure	$Bi_4Ti_3O_{12}$	Templated,[114, 115] sol-gel,[114] hydrothermal,[116] solid-state.[115]	rod,[115] tube,[114, 115] plate.[116]
	$Bi_{4-x}Nd_xTi_3O_{12}$	Templated,[117] sol-gel.[117]	tube-array[117]
	$Bi_{4-x}La_xTi_3O_{12}$	Electro-spinning,[118] sol-gel,[118] templated[119]	fibre,[118] tube[119]
	$BiFeO_3$	Templated,[120, 121] sonochemical.[122]	tubes[120], wires,[121] rod.[122]
Tungsten-Bronze	ε-WO_3	Flame spray pyrolysis[123]	particle[123]
Pyrochlore	$Bi_2T_2O_7$	Templated,[124] sol-gel.[124]	tube[124]
Non-oxides	SbSI	Vapour deposition,[125] sonochemical[126]	rod,[125] wire[126]
	$SbS_{1-x}Se_xI$	Sonochemical[127]	wire[127]
	Sb_2S_3	Templated,[128] solvent-less.[128]	wire-array[128]
	GeTe	Solution-phase synthesis[129, 130]	particle[129, 130]
Polymers	PVDF, P(VDF-TrFE)	Nano-intaglio technique,[131] nano-imprint lithography,[132-134] templated.[135-137]	ordered array,[131-133, 135] wire.[134, 136, 137]

1.4 Fabrication of Ferroelectric Nanostructures

There are two approaches for fabricating ferroelectric nanostructures: 'bottom-up' and 'top down', as highlighted in the following sections. 'Bottom-up' processing refers to the synthesis of nanomaterials starting at the atomic or molecular level. Solution-based routes, *e.g.* sol-gel based chemical solution deposition,[51, 52, 82, 88, 99, 112, 114, 117, 138] templating,[19, 51, 65-70] solution-phase decomposition[19, 53, 54, 55] and hydro/solvothermal synthesis [19, 57-63] are the most commonly employed 'bottom-up' approaches for synthesising ferroelectric nanostructures, *i.e.* nanoparticles, nanowires and nanotubes. 'Top-down' processing *e.g.* focused ion beam (FIB) milling[77-79, 108-110] and some lithographical methods such as nano-imprint lithography[92, 133, 134, 139, 140], consists of carving away at a bulk ferroelectric material to create coherently and continuously ordered nanosized structures.

1.4.1 Zero-dimensional ferroelectric nanostructures

Nanoparticles of different size and shape, such as quantum dots, spheres and cubes were the first experimentally studied ferroelectric nanostructures, due to their size-dependent ferroelectric characteristics.[29, 141, 142] Park *et al.*[29] first reported the decrease in T_C and the increase in the tetragonal crystal

distortion of $BaTiO_3$ nanoparticles with decreasing diameter (33 to 140 nm). The researchers also determined that the minimum critical diameter required for a ferroelectric phase transition in the nanoparticles was 37 nm. Since these initial findings on $BaTiO_3$ nanoparticles, many different types of ferroelectric nanoparticles have been synthesised by a variety of solution-based methods, as highlighted in the transmission electron microscopy (TEM) images shown in Figure 2.

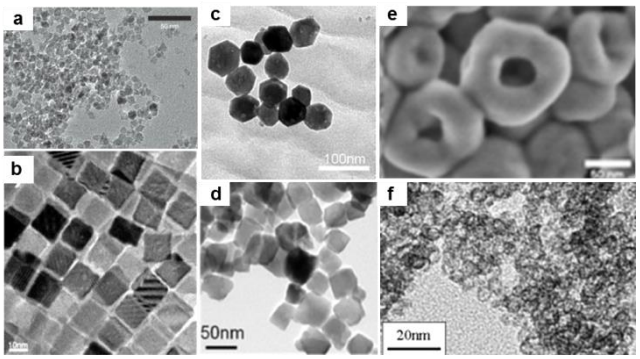

Figure 2. TEM images of (a) $BaTiO_3$ nanoparticles (~6 to 8 nm) synthesised at room temperature using a bio-inspired solution-phase metal-organic decomposition; 'Adapted with permission from Macmillan Publishers Ltd: [Nature Protocols][53] copyright (2011)', (b) $BaTiO_3$ nanocubes prepared hydrothermally; 'Adapted with permission from ref. 61, copyright 2010, American Chemical Society', (c) dodecahedral shaped $BaTiO_3$ nanoparticles prepared by hydrothermal reaction; 'Adapted with permission from ref. 60, copyright 2012, American Chemical Society', and (d) cube-shaped $LiNbO_3$ nanoparticles prepared via solvothermal route.[143] (e) SEM image of $BaTiO_3$ nanotorus prepared by hydrothermal reaction,[62] and (f) TEM image of PLZT hollow nanospheres synthesised hydrothermally; 'Adapted with permission from ref. [111], copyright 2012, Elsevier'.

Nanoparticles can be synthesised by homogeneous nucleation from a liquid phase.[36] Recently, Ould-Ely *et al.*[53] engineered the large-scale synthesis of $BaTiO_3$ nanoparticles, utilising a kinetically-controlled, vapour-diffusion-assisted hydrolysis protocol by which a bimetallic alkoxide precursor, $BaTi(OCH_2CH(CH_3)OCH_3)_6$, decomposed to produce uniform sized (~6 to 8 nm) paraelectric nanoparticles (Figure 2(a)), at room temperature; successfully yielding up to 250 ± 5 g $BaTiO_3$ nanoparticles in single batches. Sub-10 nm sized colloidal nanocrystals of germanium telluride (GeTe), the simplest known ferroelectric, was synthesised recently by the metal-organic decomposition of bis[bis(trimethylsilyl)amino]Ge(II) ($(TMS_2N)_2Ge$) with trioctylphosphine-tellurium (TOP-Te) in the presence of 1-dodecanethiol and excess trioctylphosphine at 230 °C.[129, 130] Many groups have successfully synthesised ferroelectric nanoparticles close to their predicted critical size-limit, where ferroelectricity disappears. For instance, Niederberger *et al.*[81] solvothermally prepared ultra-fine $BaTiO_3$, $SrTiO_3$, and $(Ba,Sr)TiO_3$ spherical nanoparticles with a mean diameter of 5 nm. Recently, Xu *et al.*[85] hydrothermally synthesised free-standing lead zirconate titanate (PZT) nanoparticles with diameters ~ 4 nm. Hollow ferroelectric nanostructures are also of interest; for instance, lanthanum doped lead zirconate titanate (PLZT) hollow nanospheres (Figure 2(f)) with size as low as 4 nm were prepared hydrothermally. Nanocrystals can be formed in a variety of morphologies, due to differences in the surface energy of crystal facets which are dependent on the reaction environment.[144] Thus the shape and morphology of a nanocrystal can be tuned by altering the surface-energy of a specific crystal facet by selectively adsorbing inorganic or organic ligands onto these facets.[144] This crystal engineering strategy has been successfully applied to the hydrothermal synthesis of dodecahedral shaped $BaTiO_3$ nanoparticles (Figure 2(c)), through the selective adsorption of polyethylene glycol (PEG) moieties onto the {110} surface facets of $BaTiO_3$.[60] Adireddy *et al.*[61] have also reported the controlled solvothermal synthesis of monodisperse, free-standing, $BaTiO_3$ nanocubes with a mean diameter 20 nm (Figure 2(b)). They attribute the cubical shape of the as-synthesised $BaTiO_3$ nanoparticles to the preferential formation of {100} planes during the crystal nucleation process. Similarly, cube-shaped $LiNbO_3$ nanoparticles (~50 nm in diameter, Figure 2(d)) were synthesised via solvothermal treatment of the single-source precursor, $LiNb(OEt)_6$ by Mohanty *et al.*[143]

1.4.2 One-dimensional ferroelectric nanostructures

Various types of one-dimensional (1D) semiconductor architectures[145, 146] have been already demonstrated, ranging from device configurations such as field effect transistors (FET),[147] sensors,[148] to flexible electronics components,[149] *etc.* The numerous potential applications of 1D semiconductor nanostructures arise from their geometries, which can be readily manipulated.[145, 150, 151] Recently, Weber *et al.*[152] fabricated Si nanowires with dimensions only one atom tall and four atoms wide, with remarkable low resistivity values (~0.3 mΩ. cm), comparable to the current carrying capabilities of copper.

1D ferroelectric nanostructures (nanowires, rods, tubes, belts) are the most extensively studied nanostructures due to their size-driven ferroelectric behaviour[17, 19] Among the 1D ferroelectrics, pervoskite-structured ternary oxides of ABO_3 type, *e.g.* $BaTiO_3$, $PbZr_{1-x}Ti_xO_3$, $SrTiO_3$, are the most extensively investigated material due to their excellent ferroelectric characteristics.[17, 19] Although $PbZr_{1-x}Ti_xO_3$ nanowires were the first 1D structures to be synthesised,[153, 154] $BaTiO_3$ nanowires were the first to be studied for their size-dependent ferroelectric behaviour[54, 55, 155]. Urban[55] and Yun[155] *et al.* demonstrated that $BaTiO_3$ nanowires with diameters as small as 10 nm displayed ferroelectric behaviour. Significant progress has been made recently in the synthesis and characterisation of many 1D ferroelectric nanostructures with various morphologies.[17, 19] The most commonly adopted techniques towards the realisation of 1D ferroelectrics are, 'bottom-up' routes such as template-based synthesis,[51, 82, 88, 99, 114, 120, 121] hydro/solvothermal synthesis,[59, 112, 156, 157] molten-salt synthesis,[73-76] solution-based metal-organic decomposition,[54, 55] and electrospinning[52, 118]. Among the 'top-down' approaches, methods such as focus ion beam (FIB) milling,[79] and nanoimprint lithography[91, 139, 140, 158, 159] have largely been employed. The synthesis routes to 1D ferroelectric nanostructures can be grouped into two different categories: (i) template-free synthesis, and (ii) template-assisted synthesis.

This journal is © The Royal Society of Chemistry [year]

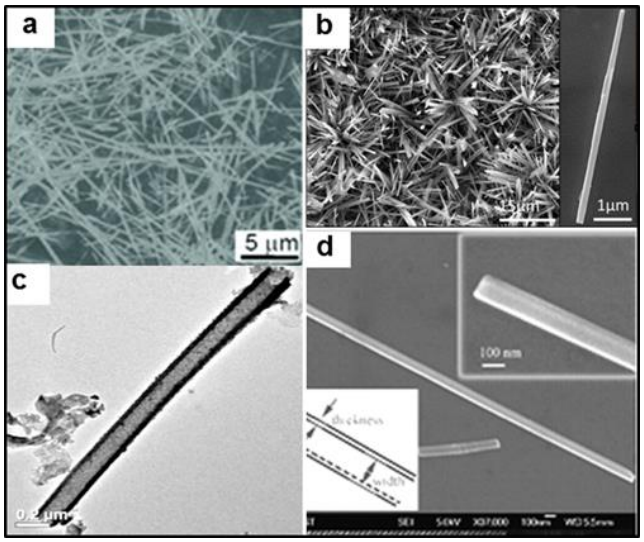

Figure 3. SEM images of (a) $NaNbO_3$ nanowires synthesised by a hydrothermal method; 'Adapted with permission from ref. [157], copyright 2011, American Chemical Society' and (b) $0.72Pb(Mg_{1/3}Nb_{2/3})O_3$-$0.28PbTiO_3$ (PMN-PT) nanowires synthesised using hydrothermal reaction (Inset shows a 5 um long single nanowire); 'Adapted with permission from ref. [160], copyright 2012, American Chemical Society'. (c) TEM image of an isolated $BaTiO_3$ nanotube made using an anodic aluminium oxide template; 'Adapted with permission from ref. 51, copyright 2009, American Chemical Society' and (d) SEM image of a $BaTiO_3$ nanostrip synthesised by a molten-salt method[73].

1.4.2.1 Template-free synthesis of 1D nanoferroelectrics

Figure 3 shows SEM and TEM images of different forms of pervoskite-based ID ferroelectric nanostructures synthesised recently by various template-free methods. Hydro/solvothermal synthesis has been effectively utilised for synthesising complex pervoskite ferroelectric nanowires and tubes, owing to the homogeneous mixing of individual reactants under subcritical conditions.[59, 112, 156, 157] This approach facilitates the easy diffusion and homogeneous nucleation of the reacting species and allows the formation of highly crystalline stoichiometric materials at low temperatures.[161] For example, highly crystalline $NaNbO_3$ nanowires (Figure 3(a)) were synthesised by the hydrothermal reaction of NaOH and Nb_2O_5 at crystallisation temperatures as low as 150 °C.[157] In hydrothermal reactions, the size, morphology and crystallinity of a material can be tuned by varying parameters such as reaction temperature, duration, solvent type, surfactant type and pH of the solution.[161] For instance, Magrez *et al.*[156] studied the evolution of 1D $KNbO_3$ nanostructures through various morphologies by adjusting the reaction temperature and concentration of the precursors used. Although hydrothermal routes for synthesising 1D nanostructures have many advantages, such as low temperature synthesis, homogeneous nucleation, narrow particle-size distribution, controlled morphology and high crystallinity, there are a number of synthetic disadvantages, which include the need for expensive autoclaves, safety issues and long reaction times. All of these drawbacks put constraints on scalability of hydrothermal methods for synthesising bulk quantities of nanoscale materials.[161]

The decomposition of metal-organic precursors in solution is another approach employed for synthesising ferroelectric nanorods and wires. Urban and co-workers[54] synthesised well-isolated single crystalline nanorods of $BaTiO_3$ and $SrTiO_3$ (diameters ranging from between 5 to 60 nm and length up to 10 µm), by the solution-phase thermolysis of barium titanium isopropoxide ($BaTi[OCH(CH_3)_2]_6$) and strontium titanium isopropoxide ($SrTi[OCH(CH_3)_2]_6$ in the presence of oleic acid respectively. The oleic acid coordinates with the precursor molecule to form an elongated inverse micelle structure in the reaction medium, which subsequently decomposed at high temperatures to form anisotropic nanorods.[54] Although organometallic decomposition methods can produce high quality 1D ferroelectric nanostructures with narrow diameter distribution, the air-sensitive nature of the precursors and relatively low product yields can be a hindrance. Another solution-based approach for producing 1D ferroelectric material is molten-salt synthesis, which has used for the large scale production of nanoferroelectrics.[73-76] This method involves the reaction of precursors in a molten salt medium, such as NaCl or KCl melt, which leads to the precipitation of the nanostructures. Molten-salt synthesis can be carried out over short time duration (1 to 4 hours) using common salts of constituent materials, making this approach more facile and environmentally benign compared to hydro/solvothermal methods.[73-76] The basic formation mechanism of nanostructures by molten-salt methods is dependent on the control of surface and interface energies of precursors and salt used; different morphologies can be formed by varying the salt or precursor concentrations.[73-76] 1D nanostructures of common ferroelectrics such as $BaTiO_3$ (Figure 3(d))[73], $SrTiO_3$, and $PbTiO_3$ have been synthesised by this method.[73-76] Electrospinning has also been used to produce high aspect ratio 1D nanofibers and wires of ferroelectric materials,[52, 105-107, 118] *e.g.* $BaTiO_3$ nanofibers[52]. Other less common techniques, such as sonochemical synthesis[126, 127, 162, 122] and electrophoretic deposition[71], have also been employed for the synthesis of ferroelectric nanowires and nanorods.

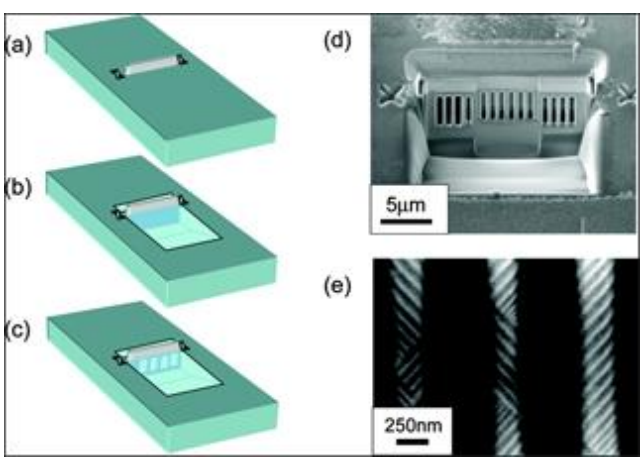

Figure 4. Schematic diagrams (a) to (c) illustrating a FIB processing method to cut nanoscale lamella into $BaTiO_3$ single-crystalline nanowires. First, a protective Pt bar is deposited by the local ion-beam induced breakdown of Pt-based organic precursor gases between two alignment crosses (a). Automated software allows the milling of trenches on either side of a $BaTiO_3$ lamella (b), and the sample is then reoriented to allow milling into the lamellar face to leave columns of material, as shown in the schematic illustration in (c). (d) SEM image of the $BaTiO_3$ columns and (e) STEM imaging using a high-angle annular dark field detector reveals distinct contrast from stripe domains. 'Reprinted with permission from ref. 79, copyright 2007, American Chemical Society'.

Ramesh *et al.*[163, 164] introduced the concept of focussed ion beam (FIB) milling for the 'top-down' fabrication of ferroelectric nanostructures. Later on, Marshall *et al.*[110] fabricated PZT nanocapacitors with surface areas ranging from 6×10^{-14} m^2 to 3×10^{-12} m^2 in the form of circular capacitors with lateral diameters between 90 nm and 2 μm using FIB milling. Schilling[79] and McQuaid[78] *et al.* adopted FIB milling technique to fabricate nanocolumns of $BaTiO_3$ from single-crystal barium titanate by a 'top-down' method (SEM images of $BaTiO_3$ nanocolumns and a detailed scheme of the FIB processing is shown in Figure 4)[79]. Although this technique is time consuming, it has the advantage of user-defined morphological control of the nanostructures produced.

1.4.2.2 Template-assisted synthesis of 1D nanoferroelectrics

In 1994 an article published in *Science*[165] by Charles R Martin highlighted the potential of using 'template-based synthetic approaches' to realise various types of nanoscopic materials, including polymers, metals and semiconductors. Template-directed 'bottom-up' synthesis has been proven as the most successful and facile strategy in making 1D ferroelectrics so far. Materials with nanosized vertical or horizontal channel structure, such as anodic aluminium oxide (AAO), track-etched polymer membranes, self-assembled block copolymer films and porous silicon, have been used as templates for synthesising 1D nanostructures.[165] The channels in the templates act as nano-moulds, whereby the precursor is impregnated into the pores of the template by suitable methods such as electrodeposition, solution or vapour phase deposition, and subsequently the precursor is decomposed to form 1D nanostructures.[165] The template can then be completely removed or partially etched to form isolated or arrays of 1D nanostructures. The major benefit associated with template synthesis is that the physical dimensions of 1D nanostructures can be precisely controlled, simply by varying the pore-diameter and length of the channels of the template employed. Moreover, monodisperse nanostructures can be harvested in large quantities owing to the high pore density (between 10^9 and 10^{12} pores per cm^2) present in the templates.[165] However, templates must meet certain processing conditions if they are to be used in the synthesis of 1D ferroelectric nanostructures, *e.g.* chemical and thermal inertness, uniformity of the porous channels and the easy release of the nanostructures from the template channels.[36, 166] In this regard, AAO templates satisfies most of the above mentioned requirements and is the most widely used template for the generation of 1D nanostructures.[167] AAO membranes have a high density of hexagonally ordered cylindrical channels (or pores) aligned perpendicular to the membrane plane (Figure 5(a-c)) and these pores can act as templates for the fabrication of 1D ferroelectric nanostructures.

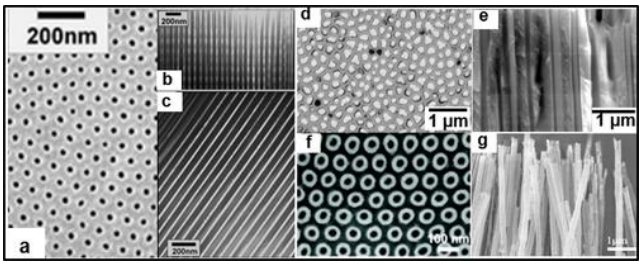

Figure 5. (a) Plan-view SEM image of an AAO template showing hexagonally ordered pores, (b) and (c) cross-sectional TEM images of same AAO memebrane showing vertically aligned pore channels; 'Adapted with permission from ref. [168], copyright 2008, American Chemical Society'. (d) Plan-view SEM image of an AAO template filled with Sb_2S_3 nanowires and (e) cross sectional SEM image of Sb_2S_3 nanowires formed inside AAO pores; 'Adapted with permission from ref. [128], copyright 2012, American Chemical Society'. (f) Plan-view SEM image of an AAO template filled with PZT nanotubes; 'Adapted with permission from ref. [102], copyright 2008, American Chemical Society' and (g) Nd-doped $Bi_4Ti_3O_{12}$ nanotubes liberated after dissolving the AAO template; 'Adapted with permission from ref. [117], copyright 2010, American Institute of Physics'.

In 2002, Hernandez *et al.*[138] explored the potential use of AAO templates to synthesise pervoskite oxide-based 1D nanostructures such as $BaTiO_3$ and $PbTiO_3$ nanotubes by a sol-gel assisted method. The method was so simple that the permeation of the precursor sol into the pores of the AAO templates was achieved by just dipping the template in the sol for 1 minute, followed by drying and calcination. Following the success of this method, many ferroelectric materials have been synthesised in 1D form by AAO templating, ranging from classic Rochelle salt[169] to many oxide based ferroelectrics (Figure 5(d-g))[51, 99, 101, 102, 104, 121, 124] and polymer ferroelectrics such as polyvinylidene difluoride (PVDF)[134, 136, 137]. Solution-based synthesis in conjunction with AAO templating is the most widely approach for producing 1D nanostructures,[51, 99, 101, 102, 121, 124] although methods such as electrodeposition[65, 71] have also been used. A Solvent-less approach has also been demonstrated to fabricate arrays of ferroelectric nanowires inside AAO template. For instance, Varghese *et al.*[128] fabricated arrays of Sb_2S_3 nanowires by melting the precursor $Sb(S_2CNEt_2)_3$ inside AAO pores. 1D nanostructures such as nanotubes, wires or rods can also act as 1D templates; either as a reactive template (where the template itself is incorporated into the final product by a suitable reaction) or a passive template (where the template is non-reactive and can be etched away after the reaction).[167] For example, TiO_2 nanowires and Bi_2O_3 nanorods have been used as reactive templates for the synthesis of $BaTiO_3$ nanowires[66] and $Bi_4Ti_3O_{12}$ nanorods/tubes[115], by treating the templates with $BaCO_3$ and a Ti(IV) peroxocomplex respectively. In a different method, PZT and $BaTiO_3$ nanotubes were prepared using passive templates such as Si and ZnO nanowires, where these sacrificial nanowire templates were etched after the deposition of the material.[170] More extensive information on the synthesis and characterisation of 1D nanoferroelectrics can be found in recent reviews by Handoko[17] and Rørvik[19] *et al.*

This journal is © The Royal Society of Chemistry [year]

1.4.3 Two-dimensional ferroelectric nanostructures

Planar structures such as plates[116] or lamella[77] and lateral arrays of nanodots[86] or wires[91] constitute the two-dimensional (2D) nanoferroelectric family. The formation of periodic arrays of isolated ferroelectric nanoislands or dots has already been shown to enhance the performance of ferroelectric random access memories (FeRAM), by providing a high density of ferroelectric single-domains per unit area.[86, 171] Different forms of 'top-down' and 'bottom-up' routes, such as electron beam lithography (EBL), nanoimprint lithography (NIL), self-assembly and template-assisted synthesis, have been used for the geometrical patterning of 2D nanoferroelectrics.

Alexe *et al.*[89] pioneered research on the 2D arrangement of ferroelectric nanostructures for their potential use in high density ferroelectric memories. The researchers used EBL for the 'top-down' fabrication of regular arrays of $SrBi_2Ta_2O_9$ and PZT nanoisland capacitors with lateral dimensions ~100 nm.[89] Huang *et al.*[90] also fabricated well-ordered PtO_x/PZT/PtO_x arrays of capacitors, down to a cell size of 90 × 90 nm, using EBL and plasma etching with a photoresist mask. Clemens *et al.*[87] have produced polycrystalline arrays of $PbTiO_3$ nanoislands (lateral dimensions ~50 to 100 nm) using EBL assisted synthesis. Nguyen and co-workers demonstrated the wafer-scale production of laterally ordered 40 nm PZT nanowires, using a 'photolithography and etching for nanoscale lithography' (PENCiL) technique.[172] This PENCiL method made use of a Ni nanowire array mask to generate horizontally aligned arrays of PZT nanowires. Dip-pen lithography[173] is another way of producing nanopatterns and was used in the fabrication of arrays of $PbTiO_3$ nanodots, with a minimum lateral dimension of ~37 nm on a Nb-doped $SrTiO_3$ substrate.[174] This method utilised the position control capabilities of an atomic force microscope (AFM) cantilever to produce patterns of ordered nanostructures.[173] Although the lithographic fabrication of nanostructures allows pre-defined precise positioning and morphological control of these structures, drawbacks such as high time consumption and complex etching process involved make it a less prevalent route for making 2D nanoferroelectrics.

NIL has emerged as a facile and high-throughput patterning technology for fabricating geometrically ordered nanostructures, in which the surface patterns of a template are replicated into a material by mechanical contact followed by de-moulding.[139] This method has the capability of achieving sub-20 nm structures with precise position.[139] The process of making arrays of wires and dots of nanostructures using a NIL method is schematically demonstrated in Figures 6(a)[91] and 6(d)[132]. Harnagea and co-workers reported seminal work on NIL processing of ferroelectric nanostructures, fabricating arrays of submicron sized (~ 300 nm) ferroelectric PZT cells.[175] Hu *et al.*[132] adopted nanoimprinting technique for the realisation of high density (~33 Gbits $inch^{-2}$) regular arrays of poly(vinylidene fluoride-trifluoroethylene) [P(VDF-TrFE)] nanocells for non-volatile memory applications (Figures 6(d) and 6(e)). Subsequently the NIL technique has been extended to fabricate arrays of PZT nanowires[91, 158] (Figures 6(c) and 6(d)) and gratings[92, 159] using sol-gel precursors. The great potential of nanoimprinting to produce a variety of geometrically ordered ferroelectric nanostructures has yet to be explored.

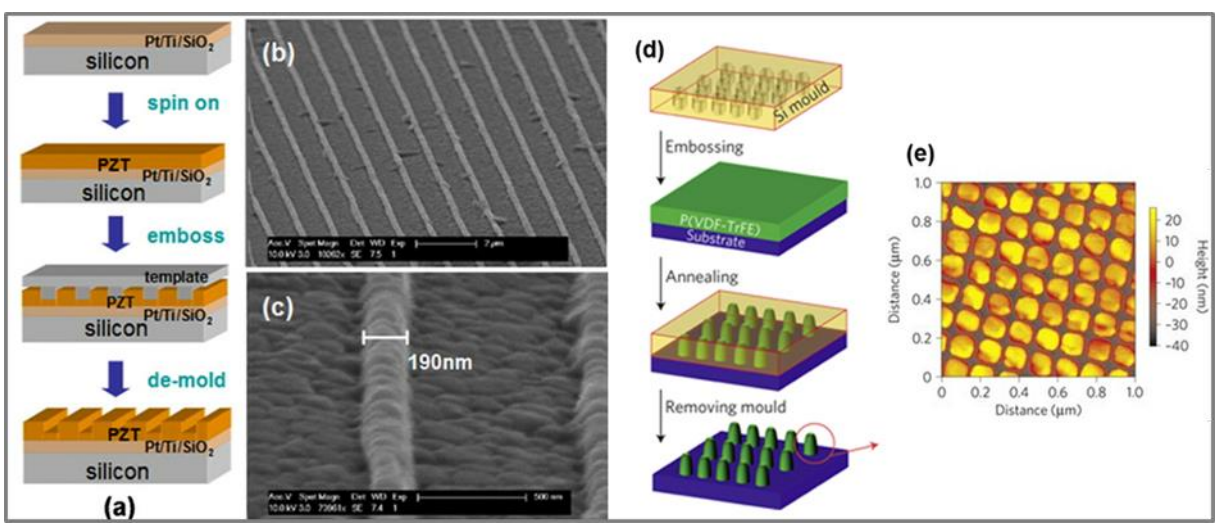

Figure 6. (a) Schematic illustration of nanoembossing process of making ferroelectric PZT nanowire arrays, (b) SEM image showing horizontally aligned PZT nanowire arrays and (c) a single PZT nanowire with width of 190 nm; 'Reprinted with permission from ref. [91], copyright 2011, Elsevier'. (d) Schematic diagram of the nanoimprinting process of P(VDF-TrFE) copolymer nanocell arrays and (e) AFM topography image of P(VDF-TrFE) copolymer nanocell arrays; 'Adapted with permission from Macmillan Publishers Ltd: [Nature Materials][132] copyright 2008'.

Among the 'bottom-up' approaches, self-assembly-based chemical solution deposition (CSD) has been regarded as the simplest route for the preparation of 2D array of ferroelectric materials.[93-98, 176] For instance, Szafraniak *et al.*[93, 96] prepared single-crystalline PZT nanoislands (20 to 200 nm in lateral dimensions) by a self-patterning CSD method based on the instability of ultrathin PZT films on a niobium-doped $SrTiO_3$ substrate. The researchers observed that the annealing temperature, substrate interface and surface defects played a crucial role in the formation of PZT nanoislands.[93-96, 176]

Although self-assembly methods have been successfully employed in making isolated ferroelectric nanostructures of smaller dimensions than those produced by optical lithography, its inability to achieve geometrical ordering and a narrow size distribution of the nanostructures make this technique less prevalent.

Template-assisted 'bottom-up' synthetic approaches provide a route to achieving 2D geometrical ordering of ferroelectric nanostructures, with narrow size distributions.[36] Nanosphere lithography (NSL)[177] has been demonstrated as a versatile template-based method for generating 2D ferroelectric nanostructures.[67-69, 103, 178-180] NSL processing consists of two steps: (i) deposition of the desired material inside the void space created by self-assembled monodisperse nanospheres, such as polystyrene latex spheres (Figure 7(a)), and (ii) dissolution of the spheres resulting in ordered arrays of 2D nanoparticles.[177] In NSL, the spacing and size of the periodically arranged nanostructures can be readily controlled by using polymer spheres with different diameters, and/or by changing the amount of material deposited,[68, 177] *e.g.* 2D patterned arrays of ferroelectric pervoskite nanodots of $BaTiO_3$ (Figure 7(b)),[67-69] PZT[179] and $SrBi_2Ta_2O_9$[67, 69], with variable dimensions and coverage density, have been created by NSL techniques in conjunction with pulsed laser deposition. In addition, NSL can be used to fabricate nanosized electrodes on top of ferroelectric thin films for producing arrays of nanoscale capacitors.[103]

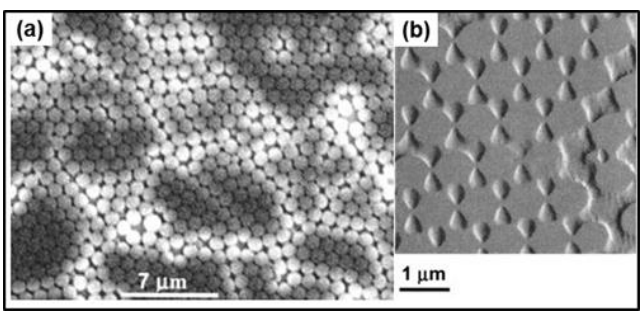

Figure 7. (a) SEM image of a hexagonally close-packed monolayer of latex spheres of 1 µm diameter and (b) contact mode AFM image (deflection image) of the well-ordered $BaTiO_3$ nanostructure made using the latex sphere template. 'Adapted with permission from ref. 67, copyright 2003, American Institute of Physics'.

Although NSL has been successful utilised for nanopatterning arrays of 2D ferroelectric materials, it is difficult to deposit multilayers of materials from the same template.[48] Since high temperature annealing is required for the crystallisation of oxide ferroelectrics, the use of polymer spheres is also not possible for multilayer deposition. These problems have been rectified by the use of thermally stable templates, such as a silicon nitride shadow mask,[181, 182] AAO membranes[86, 183, 184] and gold nanotube membranes,[185] as nanostencil masks for the fabrication of 2D arrays of nanodots. Due to the high thermal stability and inertness of these templates, they have the capability of allowing the multilayer deposition of nanomaterials. Pulsed laser deposition (PLD) has commonly been used for the controlled deposition of ferroelectric materials through nanostencil masks.[181] For example, Lee *et al.*[86] demonstrated the use of ultrathin AAO membranes as a stencil mask for the fabrication of arrays of PZT nanodots on Pt/MgO substrates by PLD. After the deposition of PZT, a layer of platinum metal was deposited on top of the nanodots, while keeping the AAO mask in place, to form Pt/PZT/Pt structures. Using this approach the researchers were able to fabricate arrays of individually addressable Pt/PZT/Pt nanocapacitors with a coverage density of 176 Gb $inch^{-2}$, for potential use in ultrahigh-density ferroelectric memories. Multilayer deposition can also be used to combine functionalities of different materials, *e.g.* Lu *et al.*[56] fabricated $BaTiO_3/CoFe_2O_4$ ferroelectric/ferromagnetic (magnetoelectric) multi-layered arrays of nanodots in order to couple the ferroelectric and ferromagnetic properties of these materials. The process of making arrays of $BaTiO_3/CoFe_2O_4$ nanodots is schematically illustrated in Figure 8.[56] AAO stencil-based nanofabrication also finds use in the patterning nanoelectrodes on ferroelectric thin films,[56] *e.g.*, $BiFeO_3$ thin film nanocapacitors have been fabricated by depositing Pt onto a 90 nm thick BFO thin film, pre-deposited on a $SrTiO_3$ substrate with a $SrRuO_3$ top electrode layer, through a AAO mask to form Pt nanoelectrodes with a thickness of 25 nm and diameter 380 nm.[186, 187]

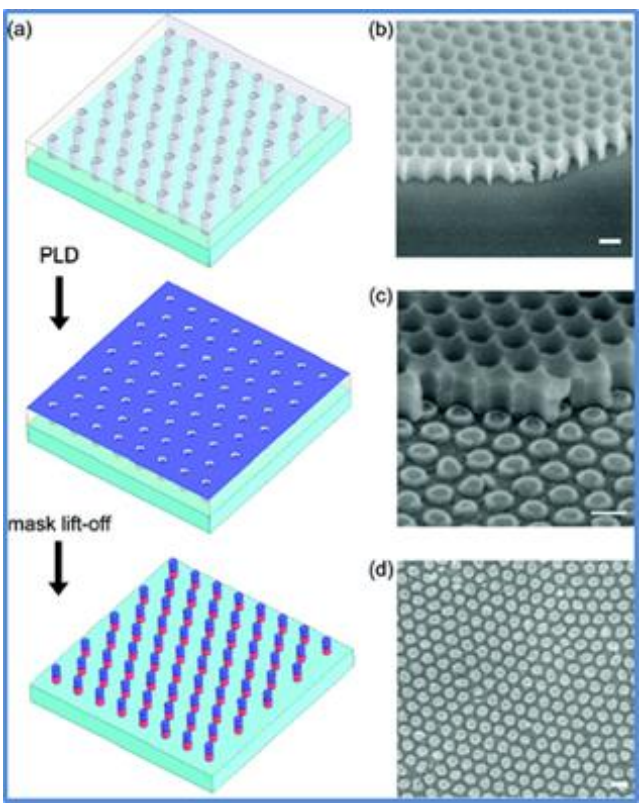

Figure 8. (a) Schematic illustration of AAO stencil-based nanofabrication of $BaTiO_3/CoFe_2O_4$ multi-layered arrays of nanodots formed by pulsed laser deposition (PLD). SEM images of (b) as-transferred AAO mask onto a STO substrate, (c) $BaTiO_3$ nanodots with partially removed AAO after first layer deposition and (d) $BaTiO_3/CoFe_2O_4$ two-layered nanodot arrays. The scale bars shown are 100 nm. 'Reprinted with permission from ref. 56, Copyright 2011, American Chemical Society'.

The self-assembly of block copolymers (BCPs) is another

This journal is © The Royal Society of Chemistry [year]

template-based fabrication route to achieve 2D ordering of nanostructures.[188, 189] Under appropriate conditions, BCPs self-assemble or phase-separate to form ordered nanoscale patterns, such as aligned cylinders and lamellas, of constituent blocks with a domain spacing that depends on the molecular weight, segment size and the strength of interaction between the polymer blocks.[188-190] BCP thin films can be transformed into nanoscale templates with well-ordered 2D patterns by selective removal of one of the constituent blocks of the copolymer[188-190]. Kang *et al.*[135] used a polystyrene-*b*-poly(ethyleneoxide) (PS-*b*-PEO) di-block polymer template for the confined crystallisation of the ferroelectric polymer PVDF-TrFE into trenches, which were 30 nm in width and 50 nm in periodicity. Kim *et al.*[100] fabricated high density array of epitaxial $PbTiO_3$ nanoislands with a height of 7 nm and a diameter of 22 nm on a single-crystalline Nb-doped $SrTiO_3$ (100) substrate over a large area (cm^2) by utilising the DSA of the polystyrene-*b*-poly(4-vinylpridine) copolymer. Recent developments in BCP-assisted patterning of nanostructures suggests that these templates have the potential to form well aligned and precisely positioned 2D patterns at sub 10 nanometre scales.[191-193] BCP-based fabrication opens up immense prospects for the production of laterally-ordered ferroelectric nanopatterns. Other techniques such as FIB processing,[77, 108, 109] single ion irradiation,[194] and solution-based synthesis[116, 129] have also used for the preparation of 2D nanoferroelectrics.

1.4.4 Three-dimensional ferroelectric nanostructures

The ability to order and align ferroelectric or piezoelectric nanostructures, especially nanotubes and nanowires, into high-density free-standing arrays is highly useful for commercial applications.[84, 195-198] For example, vertically aligned arrays of PZT nanowires (Figure 9(a)) prepared via hydrothermal synthesis, finds application as mechanical to electrical energy converters.[84] Under the application of an uniaxial compressive force, these PZT nanowires generate a piezoelectric field which in turn produces an electrical output.[84] Scott *et al.*[101] noticed intense terahertz emission from vertically aligned arrays of PZT nanotubes (Figure 9(b)), while such emission was totally absent in flat PZT films or bulk. They attributed this effect to the vertical alignment of the nanotubes.[101] Hong *et al.*[134] noticed a five times enhancement in the piezoelectric response for PVDF–TrFE nanostructures aligned perpendicular on a Si substrate compared to PVDF–TrFE thin films. 3D nanostructuring also provides an opportunity to study the size and morphology dependence of ferroelectric characteristics. For instance, Bernal and co-workers fabricated well-ordered free standing arrays of PZT nanotubes by vacuum infiltration of a sol-gel precursor solution into a polymeric template, created using electron beam lithography, and studied the effect of the critical thickness of the nanotubes on their ferroelectric behaviour.[88] Kim *et al.*[102] prepared ultra-thin-walled PZT nanotube arrays (Figure 9(c)), each with 5 nm thick walls and outer diameters of 50 nm using sol-gel infiltration of PZT precursor through AAO template pores. This template-based method[88] has the advantage of precise control over the size, shape and location of the nanostructures, enabling fabrication of NEMS and energy harvesting devices.[195]

Other methods such as hydrothermal synthesis,[199-201] PLD[202] and AAO template-assisted fabrication[99, 102, 121, 203] have also been used to prepare 3D ferroelectric nanostructures.

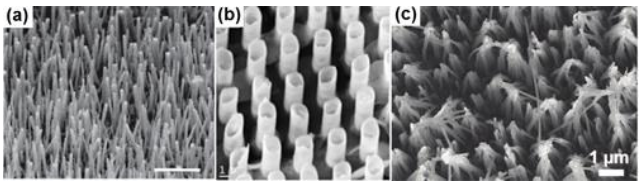

Figure 9. SEM images of (a) epitaxially grown arrays of PZT nanowires on an Nb-doped STO substrate by hydrothermal decomposition (scale bar, 5 μm); 'Adapted with permission from Macmillan Publishers Ltd: [Nature Communications][84] copyright 2010' (b) arrays of PZT nanotubes on a porous Si template produced by metalorganic-decomposition; 'Reprinted with permission from ref. [101], Copyright 2008, American Chemical Society', and (c) array of PZT nanotubes fabricated via AAO template-directed sol-gel infiltration; 'Adapted with permission from ref. [102], copyright 2008, American Chemical Society'.

1.5 Characterisation of Nanoscale Ferroelectric Materials

Although there have been numerous research articles published on the fabrication of ferroelectric nanostructures, only a few studies have focused on size-dependent ferroelectric characteristics. A significant understanding of nanoscale ferroelectricity amongst researchers evolved with the advent of scanning probe microscopy (SPM) and piezo-response microscopy (PFM) techniques.[37, 38, 204, 205] Other characterisation tools such as high resolution TEM,[79, 108, 180, 206-209] synchrotron x-ray scattering,[31] scanning probe Raman[44, 46] and dielectric spectroscopy[41-43] have also been utilised to probe scaling effects in ferroelectric nanostructures. This section will provide an overview of the latest developments in the characterisation nanoscale ferroelectrics.

PFM has been the pivotal characterisation tool for probing nanoscale materials due to its ability to locally image, quantify and manipulate ferroelectric features of individual nanostructures.[37, 38, 204, 205] PFM uses a conducting AFM tip to measure the local electromechanical response of a ferroelectric material. An applied voltage through the conducting tip on to the surface of the ferroelectric surface causes local deformation of the sample due to converse piezoelectric effects. The tip deflects in response to this deformation, which is then translated into local piezoresponse and phase images. The images obtained provide a qualitative picture of the piezoresponse and domain structure of individual nanostructures. The quantification of a piezoresponse from an individual nanostructure is possible through the application of switching-spectroscopy PFM.[39, 210] This operational mode of PFM is used to locally switch the polarisation, and acquire the resulting local switching hysteresis, of a ferroelectric nanostructure.

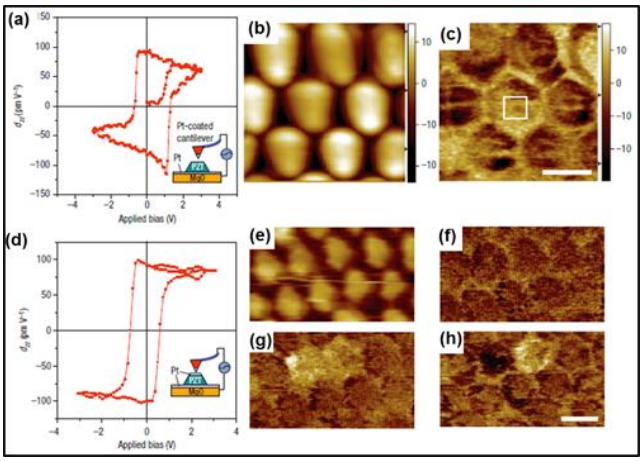

Figure 10. (a) Piezoelectric hysteresis loop obtained from epitaxially grown PZT on a Pt/MgO(100) substrate, (b) topographic and (c) piezoresponse images of nanoisland PZT/Pt/MgO(100). The hysteresis loop shown in (a) was obtained from the area marked by a white rectangle in (c). (d) Piezoelectric hysteresis loop obtained from a ferroelectric [Pt/PZT/Pt/MgO(100)] nanocapacitor, and (e) a topographic image of the corresponding sample. PFM images (f) before switching, (g) after positive switching of two capacitors by applying $+3V_{dc}$, and (h) after negative switching of one of the two previously switched capacitors by applying $-3V_{dc}$. Insets in (a) and (d) represent the switching measurement configuration. The scale bars in (b), (c) and (e–h) are 100 nm. 'Reprinted with permission from Macmillan Publishers Ltd: [Nature Nanotechnology][86], copyright 2008'.

Put together, the main uses of PFM are (i) to measure a piezo-response, (ii) ferroelectric domain imaging and patterning, (iii) to study domain dynamics and phase transformations and (iv) local polarisation switching and mapping, at the nanoscale.[33, 34, 191, 192, 211, 212] The major applications of PFM are illustrated in Figure 10 (adopted from Lee *et al.*[86]). PFM has also been used extensively to study and understand the mechanisms of nanoscale ferroelectric domain growth.[38, 204, 205, 213, 214] For example, Rodriguez *et al.* investigated the domain switching dynamics[215] and polarisation states[184] in PZT nanoislands and nanodots using PFM phase image mapping. Although PFM is a versatile and easy to use technique, its spatial resolution both in terms of PFM tip size and electric field spread, may limit its use for the smallest nanostructures of interest.[14] Recently, efforts have been made to increase the spatial resolution regime of PFM.[40, 216] Maksymovych *et al.*[40] acquired remnant piezoresponse hysteresis loops from epitaxial $BiFeO_3$ thin films with dimensions as small as 4 unit cells (1.6 nm) using PFM in ultra-high vacuum.

High-resolution TEM offers atomic-scale resolution for investigating ferroelectric polarisation domains and switching mechanisms.[79, 108, 180, 206-209] Nelson *et al.*[208] used aberration-corrected TEM combined with SPM for *in-situ* monitoring of the kinetics and dynamics of ferroelectric switching in $BiFeO_3$ thin films, at millisecond temporal and sub-Ångström spatial resolution (Figure 11). Jia *et al.*[207] used aberration-corrected TEM to study the cation–oxygen dipoles near 180° domain walls in epitaxial $PbZr_{0.2}Ti_{0.8}O_3$ thin films on the atomic scale. Similarly, Polking *et al.*[217] studied ferroelectric ordering in GeTe and $BaTiO_3$ nanocrystals (sub 10 nm) by obtaining maps of atomic-scale ferroelectric structural distortions using aberration-corrected TEM, in conjunction with holographic polarisation imaging. Gregg *et al.*[79, 111, 206] have also explored the ferroelectric domain patterns in various ferroelectric nanostructures using scanning transmission electron microscope (STEM).[79, 108, 209] Of note, the ferroelectric domain patterns and their orientations in isolated $PbZr_{0.42}Ti_{0.58}O_3$ single-crystal nanodots were visualised by means of bright-and dark-field TEM imaging.[108]

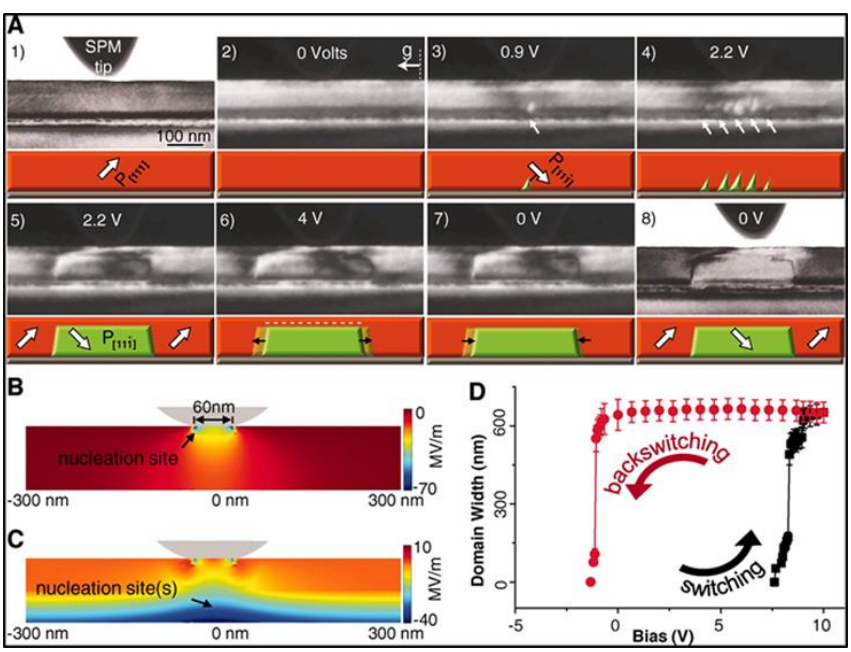

Figure 11. (A) Chronological TEM dark-field image series obtained from a single-domain $BiFeO_3$ thin film formed on a $La_{0.7}Sr_{0.3}MnO_3$ (electrode)/$TbScO_3$ substrate. Nucleation occurs at the $La_{0.7}Sr_{0.3}MnO_3$ electrode interface at 0.9 V (images 1 to 3), producing a metastable stationary

This journal is © The Royal Society of Chemistry [year]

domain. Additional bias increases the size and number of these domains up to 2.2 V (image 4). At 2.2 V, the domains merge and propagate forward just short of the surface (image 5), where they remain pinned along a (001) plane even after the voltage is nearly doubled (image 6). The lateral extent of the domain is reduced slightly with the removal of the bias (image 7) and remains unchanged after the tip is removed (image 8). (B) Normal component of the electric field from the surface probe. (C) Normal component of the electric field, including top and bottom Schottky junctions. (D) A ferroelectric hysteresis loop formed by the primary 71° switching as determined by the area of a switched domain. 'From ref. [[208]], reprinted with permission from AAAS'.

Raman spectroscopy can yield important information regarding the local crystal symmetry of a material, due to its sensitivity to atomic displacements and lattice vibrations, and thus can be used to study the domain structure and phase transition/stability in a ferroelectric material.[141, 142, 218, 219] Ultraviolet Raman spectroscopy has been used to measure to measure T_C in ultrathin films and superlattices.[220, 221] Tenne *et al.*[220] examined the size-dependence of T_C in $BaTiO_3$ films as thin as 1.6 nm using UV Raman scattering. The combination of SPM and spectroscopy techniques enables the characterisation of the structure-properties relationship of ferroelectric nanomaterials with high spatial resolution.[44] For example, Berweger *et al.*[46] used tip-enhanced Raman spectroscopy (TERS), a combination of SPM and Raman spectroscopy, to determine the crystallographic orientation and to image the ferroelectric domains in $BaTiO_3$ nanocrystals, with ~ 3 nm spatial resolution. In a similar way, scanning nonlinear dielectric microscopy (SNDM) has been used for the observation of ferroelectric polarisation distributions, domains and measurement of dielectric characteristics at nanoscale.[41-43] Non-contact mode scanning nonlinear dielectric microscopy (NC-SNDM) allows the visualisation of nanodomains and domain walls with atomic-scale resolution. In addition, SNDM has many advantages over PFM, such as high speed imaging of domains and the absence of screening effect from free surface charges.[41] All the techniques mentioned above provide an in-depth understanding of nanoscale ferroelectricity, which potentially unlocks numerous future applications for ferroelectric nanostructures.

1.6 Scaling Effects of Nanoscale Ferroelectric Materials

The scaling of a ferroelectric into 'nano' dimensions results in an increase in the materials surface area, at which point surface charges play a dominant role in determining the polarisation of the nanomaterial. 1n 1979, Kretschmer *et al.*[222] highlighted the influence of surface effects on the spontaneous polarisation of ferroelectric thin films. Thus transforming a bulk ferroelectric material into a nanostructured form can render significant changes to its characteristics, such as spontaneous polarisation (P_S), T_C and polarisation domain structure, which can be used to tune or tailor the ferroelectric features of a material.[21, 30] Moreover, nanostructuring can generate highly dense arrays of isolated ferroelectric nanostructures and domains.[86, 89, 223] Isolated domains can acts as individual memory elements for storing 'bits' of data required for high-density ferroelectric memory storage, *e.g.* Lee *et al.*[86] fabricated arrays of individually addressable Pt/PZT/Pt nanodot capacitors with a density of 176 Gb inch^{-2}, for non-volatile ferroelectric random access memory (FeRAM).

A consequence of nanostructuring ferroelectric materials is the appearance of a critical size limit, below which spontaneous polarisation cannot be sustained in a ferroelectric material.[29, 31] One cause of lost ferroelectric behaviour in nanoscale systems is the existence of a depolarising field, due to the incomplete compensation of the polarisation induced surface charges over a large surface area.[32, 224] Thus the basic understanding of this size limit in ferroelectrics is of prime importance to many potential applications,[35] since this limit determines the extent to which a ferroelectric material can be scaled down without losing its characteristics. Last decade witnessed considerable progress in investigating the critical size limit and the size influence of many ferroelectric nanostructures, of various dimensions and geometries. Even though several experimental reports on the minimum size limit of various nanoferroelectrics have been published, there have been discrepancies between the stated critical sizes, depending on the preparation route, morphology and characterisation tool used.[29, 31, 141, 142, 164, 225-229] For example, in 1988 Ishikawa and co-workers experimentally demonstrated that sol-gel-prepared $PbTiO_3$ nanoparticles displayed a critical size limit of approximately 10 nm at 300 K.[141, 142] Later on, Fong *et al.*[31] demonstrated that the ferroelectric phase in $PbTiO_3$ thin films was stable for thicknesses down to 3 unit cells (~ 1.2 nm) at room temperature. Roelofs *et al.*[98] suggested that the reduced critical size-limit of thin films could be due to the fact that they shrink the ferroelectric polarisation component in one dimension only, but not in all three directions as with nanoparticles. The critical film thickness of other pervoskite-based ferroelectrics such as $BaTiO_3$ (2.4 nm)[229] and PZT (4 nm)[226] have also been demonstrated experimentally. Apart from thin films,[31, 164, 225, 226, 229] many other nanostructured ferroelectrics have also been the subject of size-induced ferroelectric behaviour and these theoretical and experimental findings are discussed in the forthcoming section.

Zero dimensional (0D) ferroelectrics, *e.g.* nanoparticles, have been widely investigated by researchers.[29, 141, 142, 227] For example, the finite size-effect on the ferroelectric phase transitions in $PbTiO_3$ nanoparticles were studied in the late '80s.[142], *e.g.* Ishikawa *et al.*[139, 140] noticed a decrease in T_C with a decrease in the size of $PbTiO_3$ nanoparticles.[141, 142] Later in the mid '90s, Zhong[230] and Wang[231, 232] *et al.* theoretically predicted a decrease in the polarisation and T_C with decreasing particle size for $PbTiO_3$ and $BaTiO_3$ nanoparticles. Park *et al.*[29] explored the particle-size induced phase transition in $BaTiO_3$ nanoparticles, revealing that the size reduction of $BaTiO_3$ progressively increased the symmetry of its crystal structure, as evidenced by a decrease in tetragonal distortion, and consequently suppression of its ferroelectric polarisation.[29] Sun[233] and Jiang *et al.*[227] observed similar trends for $BaTiO_3$ and $PbTiO_3$ nanoparticles respectively. Jiang *et al.*[227] also noticed an increase in the dielectric constant as a function of decreasing $PbTiO_3$ particle size, attributed to the presence of an amorphous surface layer and surface energy associated with domain walls.[227] Polking *et al.*[217] revealed experimentally the influence of surface depolarisation effects on

ferroelectric polarisation stability at the nanoscale, by comparing highly conducting GeTe with strongly insulating $BaTiO_3$ nanocrystals of comparable sizes (sub 10 nm) and shapes. The polar GeTe crystals were observed to stabilise nanoscale ferroelectricity more effectively than insulating $BaTiO_3$ particles, through effective screening of polarisation-induced surface charges.[217] In addition, they demonstrated room-temperature ferroelectric polarisation switching in 10 nm $BaTiO_3$ nanocubes using PFM.[217] The concept of mechanically induced stress effects on nanoscale ferroelectrics has been reported for $BaTiO_3$ nanoparticles, by Basun *et al.*[234] Not only were $BaTiO_3$ nanoparticles observed to maintained their ferroelectric behaviour down to 10 nm, but they also showed enhanced spontaneous polarisation and dipole moment values. Numerous reports have been published to-date on the size-driven ferroelectric properties of various nanoparticles.[32, 62, 143, 209, 228, 235-238]

2D patterned arrays of ferroelectric nanoparticles, nanoislands and nanodots have been extensively studied for their scaling effect, due to their potential use in high-density FeRAM cells.[67, 69, 86, 89, 90, 140, 175, 185, 223] For example, Lee *et al.*[86] demonstrated ferroelectric switching in individual Pt/PZT/Pt nanodot capacitors with diameters of 60 nm and a height between 20–40 nm, where two neighbouring nanocapacitors could be switched into opposite states. The presence of single polarisation-domains in individual ferroelectric nanodots will be highly beneficial for the realisation of FeRAM with enhanced performance.[171] For example, Lu *et al.*[56] successfully fabricated epitaxial arrays of $BaTiO_3$ nanodots on $SrRuO_3/SrTiO_3(001)$ substrates with individual nanodots possessing single *c*-domain structures. Similar mono-domain formation was observed in arrays of $PbTiO_3$ nanodots.[100, 174, 239] Kim *et al.*[100] noted a relatively high piezoresponse in $PbTiO_3$ nanodots and attributed this enhancement to the presence of uniform sized *c*-domains. Son and co-workers explored the size-dependent ferroelectric behaviour in $PbTiO_3$ nanodots.[174, 239] They noted a decrease in the piezoelectric coefficient (d_{33}) and an increase in the coercive electric field with decreasing thickness, or increasing lateral size, of the nanodots and illustrated that $PbTiO_3$ nanodots with diameter around 10 nm could preserve ferroelectricity.[174, 239] Similar trend in ferroelectric behaviour was also reported by Kim *et al.*[100] Ma *et al.*[69] demonstrated the retention of ferroelectricity in arrays of $BaTiO_3$ nanocrowns and $SrBi_2Ta_2O_9$ nanorings with dimensions as small as ~9 and 5 nm, respectively. Chu *et al.*[94] studied the role of substrate-ferroelectric interfaces on the size-driven ferroelectricity in epitaxially grown PZT nanoislands on $SrTiO_3(001)$ substrates. They highlighted that individual PZT nanoislands, with a height of ~10 nm, displayed ferroelectric polarisation instability associated with misfit dislocations between the PZT lattice and the substrate.

Significant progress has been achieved in understanding the scaling effects in 1D ferroelectrics, especially nanowires. Yun[155] and Urban *et al.*[55] provided the seminal experimental evidence for the presence of ferroelectricity in individual $BaTiO_3$ nanowires as small as 10 nm in diameter, using scanning probe microscopy. Moreover, they demonstrated the non-volatile memory application potential of these nanowires by locally switching ferroelectric polarisation domains in these structures, as small as 100 nm^2.[155] Also, Suyal *et al.*[240] studied nanoscale ferroelectric behaviour in potassium niobate tantalate $[K(Nb_{0.8}Ta_{0.2})O_3]$ nanorods using PFM and were successful at switching the polarisation direction of an area of 50 nm^2 on an individual nanorod. Many theoretical investigations were subsequently undertaken to elucidate ferroelectric behaviour in 1D nanoferroelectrics. For instance, Naumov and Fu theoretically predicted the existence of ferroelectric ordering in PZT nanowires with diameters larger than 2 nm.[241] They also concluded that the 1D morphology of nanowires may force the polarisation to align either along the longitudinal or the transverse direction, depending on the extent of the depolarisation field in that particular direction.[241] Thus the diameter of a ferroelectric nanowire may be used to tune the magnitude of spontaneous polarisation and T_C.[241] Also, Hong *et al.*[34] demonstrated theoretically that T_C, the mean polarisation and the area of ferroelectric hysteresis loops decreases upon reducing the diameter of $BaTiO_3$ nanowires (Figure 12) and the ferroelectricity in these wires disappears at a critical size of ~ 1.2 nm,[34] consistent with the prediction by Geneste *et al.*[33]

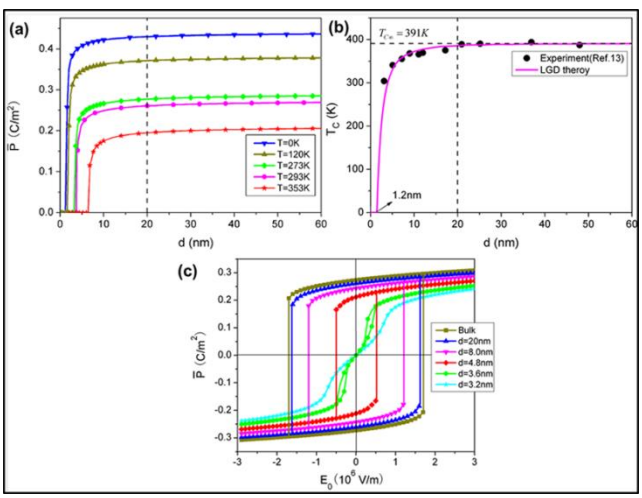

Figure 12. Size effects on (a) the mean polarisation at different temperatures, (b) T_C (black dots are from experiment[242]) and (c) polarisation-electric field (*P*-*E*) hysteresis loops (T = 293 K) of $BaTiO_3$ nanowires. 'Adapted with permission from ref. 34, copyright 2008, American Institute of Physics'.

Moreover, Spanier *et al.*[242] proved experimentally that T_C in $BaTiO_3$ nanowires was inversely proportional to the nanowire diameter. They noticed that T_C fell below room temperature at a nanowire diameter ~ 3 nm,[242] while bulk $BaTiO_3$ samples show a T_C of 120 °C.[8, 243] An extrapolation of this data indicated that $BaTiO_3$ nanowires with diameter as small as 0.8 nm can support ferroelectricity at lower temperatures. They explained the observed ferroelectric stability at lower nanowire diameters by an adsorbate-induced charge screening mechanism, by which the depolarisation field can be minimised; for instance, by surface hydroxyl (-OH) groups. In addition, their theoretical calculations indicated that the ferroelectric polarisation can be tuned by changing the surface properties of the nanowire, which opened up new possibilities in controlling ferroelectricity at the molecular level.[244, 245] Li and co-workers studied the polarisation-dependence of physisorption on ferroelectric surfaces.[245] They

This journal is © The Royal Society of Chemistry [year]

investigated the energetics of physisorption on ferroelectric domains for CH_3OH and CO_2 on $BaTiO_3$ and $Pb(Ti_{0.52}Zr_{0.48})O_3$ thin film surfaces, with the aim of tailoring surface reactivity. Recently, Louis *et al.*[246] demonstrated experimentally that the direction and extent of ferroelectric polarisation in a ferroelectric nanowire can be tuned by varying its size. They conducted their study on $KNbO_3$ and $BaTiO_3$ nanowires using a combination of experimental and theoretical techniques, such as X-ray diffraction, Raman spectroscopy and first-principles-calculation, to reveal the nanoscale ferroelectric phase transition mechanism. Also, Schilling and co-workers demonstrated morphologically-controlled ferroelectric polarisation in single-crystal $BaTiO_3$ nanowires, by locally changing the aspect ratio of the nanowires using FIB milling techniques.[79] They noticed the presence of axial (∥ to the nanowire axis) and non-axial (⊥ to the axis) polarisation components in these nanowires, which were strongly sensitive to the local morphology.

Any fabrication technique that can easily manipulate the size and dimensions of ferroelectric nanowires offers great advantages for studying the scaling effect. From this viewpoint, template-based fabrication techniques need special mention. Preferential crystal orientation, ordering and high-density arrays of ferroelectric nanostructures can be achieved by templating.[70, 88, 99, 102, 104, 117, 169, 198] Since ferroelectricity is a co-operative phenomenon, crystal orientation and ordering have a significant influence on the ferroelectric properties of nanoscale materials, such as polarisation direction and domain structure. Recently, Bernal *et al.*[88] fabricated highly-ordered vertical arrays of PZT nanotubes with variable diameters, using an EBL-patterned polymeric electron resist template, to study piezoelectric size effects. The size effect in the PZT nanotubes with various wall thicknesses, ranging from 5 nm to 25 nm, was studied while keeping the aspect ratio constant. They noticed an increase in the remnant piezoresponse and a decrease in coercive voltage with increasing tube wall thickness and also the presence of a critical size limit at ~ 10 nm. Yadlovker *et al.*[169] prepared highly dense array of Rochelle salt (RS) single crystalline nanorods with uniform ferroelectric polarisation orientation and nanodomain sizes using AAO templates. These arrays of nanowires exhibited an enhancement in their spontaneous polarisation, one order higher than reported for bulk RS, due to the single crystalline nature and long-range ordering of the wires inside the AAO membranes. Similar enhancements have been reported for single crystalline KIO_3, [247] Sb_2S_3 [128] and $PbTiO_3$ [200, 201] nanorods. As noted above, preferential orientation of ferroelectric nanostructures can enhance ferroelectricity by introducing anisotropy in a particular direction. Vertically aligned PVDF−TrFE co-polymer nanograss structures showed a piezoelectric response (210.4 pm V^{-1}) five times larger than that of its flat thin film counterparts.[134] Similar enhancements in piezoelectric performance were observed in horizontally aligned arrays of PZT nanowires, where the nanowires displayed the highest reported piezoelectric coefficient (d_{eff} ~145 pm V^{-1}) reported,[172] as well as in arrays of buckled PZT nanoribbons.[248] More in depth information on scaling effects in nanoscale ferroelectrics can found in recently published reviews.[14, 16, 19]

1.7 Applications of Nanoscale Ferroelectric Materials

The polarisation of ferroelectric materials can be changed by using three forms of energy, *i.e.* electric, thermal and mechanical or vice versa, giving these materials pyroelectric and piezoelectric characteristics as well. These three inter-dependent properties of ferroelectrics have been widely exploited for many functional applications.[11, 243, 249, 250] The various applications of ferroelectrics are schematically shown in Figure 13. The reversible polarisation of a ferroelectric material can be used in non-volatile memory applications, as the direction of polarisation switching represents the binary '1' and '0' in data storage.[11, 243, 250, 251] Ferroelectric thin films have already shown potential as FeRAMs in memory storage applications.[11, 243, 250] The piezo effect in ferroelectrics can be used to convert mechanical energy to electrical energy, or vice versa, and find wide-spread use as actuators, transducers and micro-elelctromechanical (MEMS) devices.[11] As all ferroelectric materials are pyroelectric, they can also generate an electrical current in response to any change in ambient temperature; this principle finds use in infrared thermal imaging.[10, 252] In addition, pyroelectric materials can act as energy scavengers,[253] whereby electrical energy can be created from wasted heat in an electronic circuit.[254] Owing to their high dielectric permittivity, ferroelectrics also find extensive use as capacitors in electronic industry.[11, 243, 249] Apart from the niche applications mentioned above, the latest developments in the use of nanoferroelectrics are summarised in the following section.

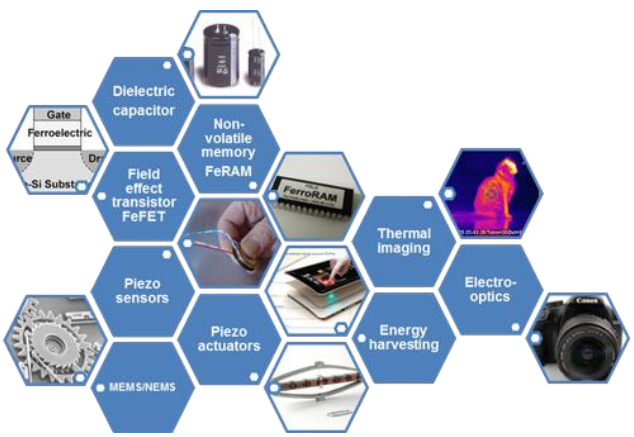

Figure 13. Application ranges of ferroelectric, piezoelectric and pyroelectric materials.

Significant efforts have been made recently to achieve high efficiency ferroelectric memory devices, through the assistance of nanostructuring.[13, 18, 20, 86, 89, 135, 198, 255-259] Different types of nanodevice architectures with improved features have been realised, based on the reversible polarisation of the ferroelectrics, *e.g.* switchable remnant polarisation in a ferroelectric material is applied in FeRAM.[251] By scaling down the size of individual memory cells, the storage efficiency of FeRAMs can be greatly improved.[86] Shen *et al.*[159] explored the potential application of horizontally-aligned arrays of PZT nanowires for multi-bit storage applications. In addition, the ferroelectric polarisation can be coupled directly to the channel of a field effect transistor (FET), to form ferroelectric FET or FeFET, in which the direction

of the polarisation determines the on-off state of the device.[13, 259] Recently there has been significant interest in nanostructured ferroelectric polymers, especially PVDF-TrFE copolymers, for non-volatile memory cells owing to their cost effective production and inherent flexibility.[133, 135, 257, 258] For example, PVDF-TrFE based FeFETs with enhanced memory features were realised by nano confinement of the polymer within self-assembled organosilicate lamellae.[135] The reversible polarisation of ferroelectric materials could also be used to change the charge injection/transport properties of the material, and has the potential for memory storage.[12, 18] A ferroelectric tunnel junction (FTJ) is working on this principle, where the electrical resistance at a FTJ can be tuned using orientation of ferroelectric polarisation.[13, 18, 206, 256, 260-264] Chanthbouala *et al.*[256] have demonstrated FTJ-based solid state memory with high off/on ratios (100), and very low write power (~ 1×10^4 A cm^{-2}) using a 2 nm $BaTiO_3$ thin film (Figure 14).

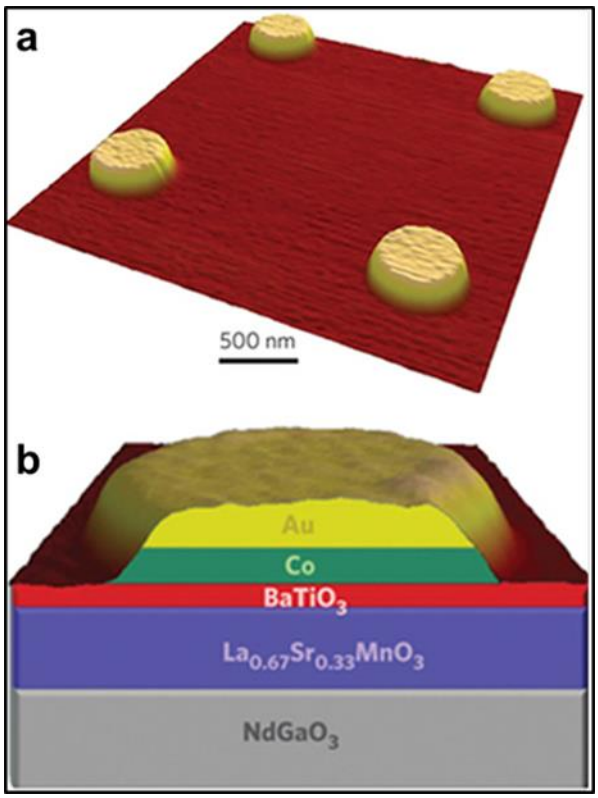

Figure 14. (a) AFM image of four typical FTJ nanodevices defined using electron-beam lithography. (b) Schematic of a gold (10 nm)/cobalt (10 nm)/$BaTiO_3$ (2 nm)/$La_{0.67}Sr_{0.33}MnO_3$ (30 nm) nanodevice on a (001) $NdGaO_3$ single-crystal substrate. 'Reprinted with permission from Macmillan Publishers Ltd: [Nature Nanotechnology][256], copyright 2011'.

Piezoelectric nanostructures, especially nanowires, have been studied extensively for their potential energy harvesting capabilities from collective mechanical movements.[84, 107, 195, 196, 248, 265-267] This area of research called piezotronics was first introduced by Zhong Lin Wang.[195] Electrical energy collected from piezoelectric nanostructures has already been utilised effectively to power nanoelectronics devices[84] and sensors[196]. 1D nanostructures, especially nanowires and rods, have mostly been used for piezotronics applications due to their large mechanical strain tolerance.[195] In particular, vertically or horizontally aligned arrays of piezoelectric nanowires are in an ideal configuration for energy harvesting applications due to their enhanced anisotropic piezo-response.[84, 107, 195, 196, 248, 265-267]

This journal is © The Royal Society of Chemistry [year]

Cite this: DOI: 10.1039/c0xx00000x

www.rsc.org/xxxxxx

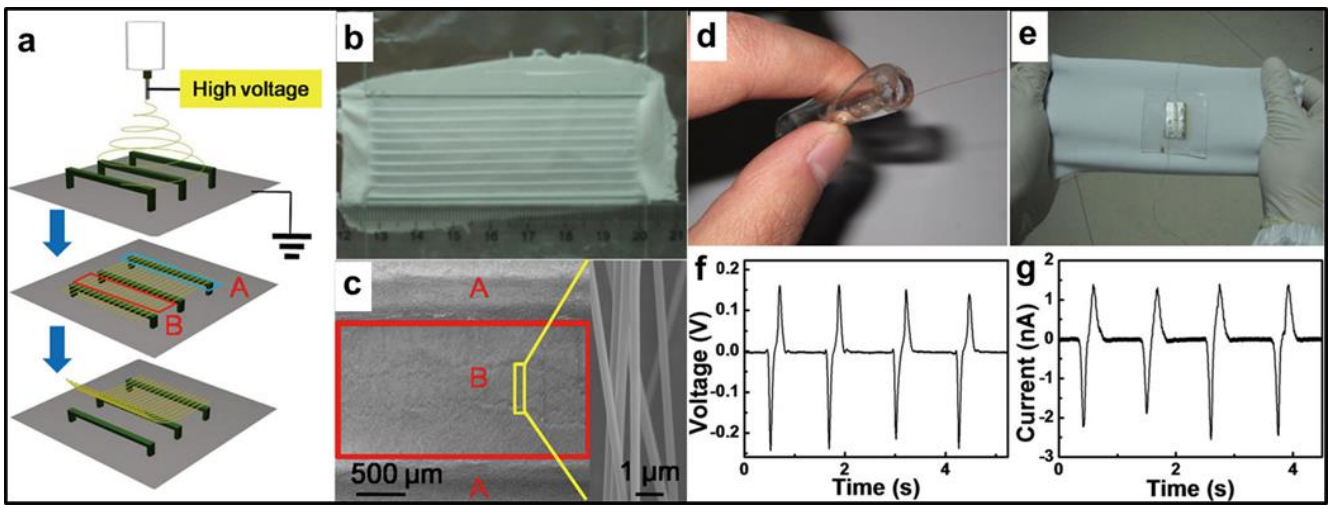

Figure 15. (a) Schematic diagram of the electrospinning process of fabricating a PZT textile. (b) and (c) Photograph and SEM images of the PZT textile, respectively. (d) Photograph of a tube bent with a substrate-free PZT textile nanogenerator, which shows its flexibility. (e) Working mode of a wearable nanogenerator; the stretching and releasing of the chemical fabric can drive the nanogenerator. (f) and (g) Output open-circuit voltage and short-circuit current of a wearable nanogenerator, respectively. 'Adapted with permission from ref. [107], copyright 2012, American Chemical Society'.

Xu *et al.*[84] demonstrated the use of vertically aligned arrays of PZT nanowires to generate electricity from random mechanical movements of the wires. The nanogenerators fabricated using the arrays of PZT nanowires produced a peak output voltage of ~0.7 V, a current density of 4 μA cm^{-2} and an average power density of 2.8 mW cm^{-3}; this harvested electrical energy was used to power a commercial laser diode and demonstrates the great potential of piezotronics as a potential self-power source for touch sensitive personal devices. The flexibility and stretchability of piezoelectric nanostructures adds extra functionality and efficiency to energy harvesting systems.[107, 248, 266, 267] Wu *et al.*[107] fabricated flexible and wearable nanogenerators using PZT nanowires embedded in a polymer and a textile matrix, respectively (Figure 15) and this nanogenerator produced an output voltage and current of 6 V and 45 nA respectively. An alternative approach for ferroelectric-based energy harvesting is based on pyroelectric properties.[253, 254, 268] Pyroelectric energy conversion offers a way to convert waste heat directly into electricity and can be potentially used to scavenge heat from electronic circuit boards.[253, 254]

Most of the applications mentioned above make use of either thin films or 1D ferroelectric nanostructures. Isolated ferroelectric nanoparticles also find use in a wide range of applications. For example, ferroelectric nanoparticles find extensive use as a filler material in polymer-nanocomposite based structures.[236, 269] $BaTiO_3$ nanoparticle-based polymer nanocomposites are widely studied. Isolated super-paraelectric $BaTiO_3$ and $(Ba,Sr)TiO_3$ nanoparticles (8-12 nm) synthesised via a solvothermal process find use as a functional filler material in polymer composite based organic field effect transistors (OFETs).[236] Surface functionalisation is another active area of interest for ferroelectric nanoparticles.[270] Owing to the high surface energy of nanoparticles, their functionalisation using suitable organic moieties can add tunability to the dielectric and functional characteristics of ferroelectric nanocrystals.[244] In addition, the dispersion of ferroelectric nanoparticles in a polymer matrix can be improved by proper modification of the surface of ferroelectric nanoparticles, which in turn provides enhanced dielectric characteristics to the polymer nanocomposite.[269, 271-273] Ferroelectric nanoparticle-filled polymer nanocomposites have also shown potential in applications such as dielectric energy storage, flexible thin-film dielectric capacitors[269, 271-273] and flexible electrical energy generators[274].

1.8 Future Outlook of Nanoscale Ferroelectric Materials

The prospect for nanoscale ferroelectric materials is promising, as evident from the growing research articles in theory, fabrication and application aspects of these structures.[13, 15-20, 48, 50, 86, 135] A basic understanding of the finite-size effect in nanoscale ferroelectric is a prerequisite for the development of new devices and hence more theoretical studies in this area would be highly advantageous. Fabrication routes that have the capability of generating nanostructured patterns with predictable shapes and controlled dimensions, at desired locations on a substrate of interest, are critical for the integration of novel nanoferroelectric devices. For instance, the potential use of nanoimprint

lithography[91, 139, 140, 159] and self-assembled BCPs[191, 193, 275] to produce highly ordered patterns of nanostructures could be effectively exploited to achieve the above mentioned challenges. Efforts in enhancing the spatial resolution of current characterisation tools will also be required to tackle the future developments in nanoscale ferroelectric research.[40, 44, 216] Characterisation techniques such as PFM, SNDM,[41-43] TERS[44, 46] and TEM[108, 207, 208, 217] require special mention in this regard. The broad application spectrum of nanoscale ferroelectric materials spanning from memory devices to self-powered nanogenerators may fuel future interests in research and developments in this area. Progress in controlling ferroelectricity on the nanoscale offers great potential for nanoscale ferroelectric devices, especially FeFETs and FTJs.[16, 185, 245, 246, 251-255] The 2011 international technology road map for semiconductors (ITRS) has listed ferroelectric-based FTJs and FeFETs as two emerging memory technologies.[12] Moreover, the still advancing area of piezotronics offers immense possibilities in the creation of efficient self-powered microelectronic devices.[84, 107, 195, 196, 248, 266, 267]

Acknowledgment

The authors acknowledge the financial support from Science Foundation Ireland (SFI) under the FORME Strategic Research Cluster Award (Project 07/SRC/I1172) and also the Higher Education Authority Program for Research in Third Level Institutions (2007-2011) via the INSPIRE program.

Notes and references

[*a] *Materials Chemistry and Analysis Group, Department of Chemistry, University College Cork, Cork, Ireland. Fax: +353 21 427 4097; Tel: +353 21 4903608; E-mail: j.holmes@ucc.ie*

[b] *Tyndall National Institute, University College Cork, Lee Maltings, Dyke Parade, Cork, Ireland.*

[c] *Centre for Research on Adaptive Nanostructures and Nanodevices (CRANN), Trinity College Dublin, Dublin 2, Ireland.*

References

1. J. Curie and P. Curie, *Comptes Rendus de l'Académie des Sciences*, 1880, **91**, 294 - 295.
2. J. Curie and P. Curie, *C R Acad Sci Gen.*, 1880, **91**, 383 - 386.
3. J. Valasek, *Ferroelectrics*, 1971, **2**, 239-244.
4. E. Schrödinger, *S.B. Akad. Wiss. Wien*, 1912, **121**, 1937-1972.
5. J. Valasek, *Physical Review*, 1921, **17**, 475.
6. J. Fousek, *Proceedings of the Ninth IEEE International Symposium on Applications of Ferroelectrics, ISAF '94.*, 1994, 1-5.
7. L. E. Cross and R. E. Newnham, in *High technology ceramics: past, present, and future : the nature of innovation and change in ceramic technology*, eds. W. D. Kingery and E. Lense, American Ceramic Society, Westerville, OH, 1986, vol. III, pp. 289-305.
8. A. Vonhippel, R. G. Breckenridge, F. G. Chesley and L. Tisza, *Ind. Eng. Chem.*, 1946, **38**, 1097-1109.
9. T. Mitsui, in *Springer Handbook of Condensed Matter and Materials Data*, eds. W. Martienssen and H. Warlimont, Springer Berlin Heidelberg, 2005, pp. 903-938.
10. M. E. Lines and A. M. Glass, in *Principles and Applications of Ferroelectrics and Related Materials*, Oxford University Press, Oxford, 1977.
11. G. H. Haertling, *J. Am. Ceram. Soc.*, 1999, **82**, 797-818.
12. *The International Technology Roadmap for Semiconductors: 2011 Edition, Emerging research materials and Emerging research devices;* *http://www.itrs.net/Links/2011ITRS/2011Chapters/2011ERM.pdf*, *http://www.itrs.net/Links/2011ITRS/2011Chapters/2011ERD.pdf*.
13. M. Bibes, *Nat Mater*, 2012, **11**, 354-357.
14. J. M. Gregg, *physica status solidi (a)*, 2009, **206**, 577-587.
15. A. Gruverman and A. Kholkin, *Rep. Prog. Phys.*, 2006, **69**, 2443.
16. H. Han, Y. Kim, M. Alexe, D. Hesse and W. Lee, *Adv. Mater.*, 2011, **23**, 4599-4613.
17. A. D. Handoko and G. K. L. Goh, *Science of Advanced Materials*, 2010, **2**, 16-34.
18. A. M. Ionescu, *Nat Nano*, 2012, **7**, 83-85.
19. P. M. Rørvik, T. Grande and M.-A. Einarsrud, *Adv. Mater.*, 2011, **23**, 4007-4034.
20. J. F. Scott, F. D. Morrison, M. Miyake and P. Zubko, *Ferroelectrics*, 2006, **336**, 237-245.
21. N. A. Spaldin, *Science*, 2004, **304**, 1606-1607.
22. K. C. Kao, in *Dielectric Phenomena in Solids*, Academic Press, San Diego, 2004, pp. 213-282.
23. in *Landolt-Börnstein - Group III Condensed Matter*, eds. Y. Shiozaki, E. Nakamura and T. Mitsui, Springer-Verlag, 2002, vol. III/36a-c.
24. R. Weil, R. Nkum, E. Muranevich and L. Benguigui, *Phys. Rev. Lett.*, 1989, **62**, 2744-2746.
25. E. Fatuzzo, R. Nitsche, G. Harbeke, W. Ruppel, H. Roetschi and W. J. Merz, *Physical Review*, 1962, **127**, 2036-2037.
26. A. J. Lovinger, *Science*, 1983, **220**, 1115-1121.
27. K. Kinam, J. Gitae, J. Hongsik and L. Sungyung, *Proceedings of the IEEE 2005 Custom Integrated Circuits Conference.*, 2005, 423-426.
28. D. Fischer, in *connectingindustry.com/electronics*, 2010, vol. September 2010, pp. 22-23.
29. P. Yung, L. Won-Jae and K. Ho-Gi, *J. Phys.: Condens. Matter*, 1997, **9**, 9445.
30. C. H. Ahn, K. M. Rabe and J.-M. Triscone, *Science*, 2004, **303**, 488-491.
31. D. D. Fong, G. B. Stephenson, S. K. Streiffer, J. A. Eastman, O. Auciello, P. H. Fuoss and C. Thompson, *Science*, 2004, **304**, 1650-1653.
32. I. I. Naumov, L. Bellaiche and H. Fu, *Nature*, 2004, **432**, 737-740.
33. G. Geneste, E. Bousquet, J. Junquera and P. Ghosez, *Appl. Phys. Lett.*, 2006, **88**, 112906.
34. J. Hong and D. Fang, *Appl. Phys. Lett.*, 2008, **92**, 012906.
35. B. Vilquin, B. Gautier, A. Brugere and J. S. Moulet, *AIP Conference Proceedings*, 2009, **1173**, 129-134.
36. G. Cao, *Nanostructures and Nanomaterials : Synthesis, Properties, and Applications*, 1 edn., Imperial College Press, London, 2004.
37. S. Elisabeth, *J. Phys. D: Appl. Phys.*, 2011, **44**, 464003.
38. N. Balke, I. Bdikin, S. V. Kalinin and A. L. Kholkin, *J. Am. Ceram. Soc.*, 2009, **92**, 1629-1647.
39. S. Jesse, H. N. Lee and S. V. Kalinin, *Rev. Sci. Instrum.*, 2006, **77**, 073702.
40. P. Maksymovych, M. Huijben, M. Pan, S. Jesse, N. Balke, Y.-H. Chu, H. J. Chang, A. Y. Borisevich, A. P. Baddorf, G. Rijnders, D. H. A. Blank, R. Ramesh and S. V. Kalinin, *Phys Rev B*, 2012, **85**, 014119.
41. K. Tanaka, Y. Kurihashi, T. Uda, Y. Daimon, N. Odagawa, R. Hirose, Y. Hiranaga and Y. Cho, *Jpn J Appl Phys*, 2008, **47**, 3311-3325.
42. Y. Cho, *J. Mater. Res.*, 2011, **26**, 2007-2016.
43. Y. Cho, S. Kazuta and K. Matsuura, *Appl. Phys. Lett.*, 1999, **75**, 2833-2835.
44. M. Lucas and E. Riedo, *Rev. Sci. Instrum.*, 2012, **83**, 061101-061135.
45. P. Verma, T. Ichimura, T. Yano, Y. Saito and S. Kawata, *Laser & Photonics Reviews*, 2010, **4**, 548-561.
46. S. Berweger, C. C. Neacsu, Y. Mao, H. Zhou, S. S. Wong and M. B. Raschke, *Nat Nano*, 2009, **4**, 496-499.
47. V. V. Pokropivny and V. V. Skorokhod, *Materials Science and Engineering: C*, 2007, **27**, 990-993.
48. I. Vrejoiu, M. Alexe, D. Hesse and U. Gösele, *Adv. Funct. Mater.*, 2008, **18**, 3892-3906.
49. I. Vrejoiu, M. Alexe, D. Hesse and U. Gosele, *Journal of Vacuum Science & Technology B*, 2009, **27**, 498-503.
50. X. Zhu, *Recent Patents on Nanotechnology*, 2009, **3**, 42-52.

This journal is © The Royal Society of Chemistry [year]

51. Y.-Y. Chen, B.-Y. Yu, J.-H. Wang, R. E. Cochran and J.-J. Shyue, *Inorg. Chem.*, 2008, **48**, 681-686.
52. H. Li, H. Wu, D. Lin and W. Pan, *J. Am. Ceram. Soc.*, 2009, **92**, 2162-2164.
53. T. Ould-Ely, M. Luger, L. Kaplan-Reinig, K. Niesz, M. Doherty and D. E. Morse, *Nat. Protocols*, 2011, **6**, 97-104.
54. J. J. Urban, W. S. Yun, Q. Gu and H. Park, *J. Am. Chem. Soc.*, 2002, **124**, 1186-1187.
55. J. J. Urban, J. E. Spanier, L. Ouyang, W. S. Yun and H. Park, *Adv. Mater.*, 2003, **15**, 423-426.
56. X. Lu, Y. Kim, S. Goetze, X. Li, S. Dong, P. Werner, M. Alexe and D. Hesse, *Nano Lett.*, 2011, **11**, 3202-3206.
57. W. Sun, Y. Pang, J. Li and W. Ao, *Chem. Mater.*, 2007, **19**, 1772-1779.
58. U. A. Joshi and J. S. Lee, *Small*, 2005, **1**, 1172-1176.
59. Y.-F. Zhu, L. Zhang, T. Natsuki, Y.-Q. Fu and Q.-Q. Ni, *ACS Applied Materials & Interfaces*, 2012, **4**, 2101-2106.
60. H. Zhan, X. Yang, C. Wang, J. Chen, Y. Wen, C. Liang, H. F. Greer, M. Wu and W. Zhou, *Cryst Growth Des*, 2012, **12**, 1247-1253.
61. S. Adireddy, C. Lin, B. Cao, W. Zhou and G. Caruntu, *Chem. Mater.*, 2010, **22**, 1946-1948.
62. F. Xia, J. Liu, D. Gu, P. Zhao, J. Zhang and R. Che, *Nanoscale*, 2011, **3**, 3860-3867.
63. J. Yang, B. Geng, Y. Ye and X. Yu, *CrystEngComm*, 2012, **14**, 2959-2965.
64. Y. Hakuta, H. Ura, H. Hayashi and K. Arai, *Industrial & Engineering Chemistry Research*, 2005, **44**, 840-846.
65. D. H. Edward, A. P. Nicholas, D. H. Bryan and P. P. Nitin, *Nanotechnology*, 2010, **21**, 335601.
66. M. Teresa Buscaglia, C. Harnagea, M. Dapiaggi, V. Buscaglia, A. Pignolet and P. Nanni, *Chem. Mater.*, 2009, **21**, 5058-5065.
67. W. Ma, C. Harnagea, D. Hesse and U. Gosele, *Appl. Phys. Lett.*, 2003, **83**, 3770-3772.
68. W. Ma, D. Hesse and U. Gösele, *Small*, 2005, **1**, 837-841.
69. M. Wenhui, H. Dietrich and G. Ulrich, *Nanotechnology*, 2006, **17**, 2536.
70. Y. Luo, I. Szafraniak, V. Nagarajan, R. B. Wehrspohn, M. Steinhart, J. H. Wendorff, N. D. Zakharov, R. Ramesh and M. Alexe, *Integrated Ferroelectrics*, 2003, **59**, 1513-1520.
71. Ž. Kristina, H.-R. Francisco, P. Joan Daniel, M. Joan Ramon, R. Aleksander and Č. Miran, *Nanotechnology*, 2011, **22**, 385501.
72. F. Maxim, P. Ferreira, P. M. Vilarinho, A. Aimable and P. Bowen, *Cryst Growth Des*, 2010, **10**, 3996-4004.
73. H. Deng, Y. Qiu and S. Yang, *J. Mater. Chem.*, 2009, **19**, 976-982.
74. Y. Mao, S. Banerjee and S. S. Wong, *J. Am. Chem. Soc.*, 2003, **125**, 15718-15719.
75. Z. Cai, X. Xing, R. Yu, X. Sun and G. Liu, *Inorg. Chem.*, 2007, **46**, 7423-7427.
76. P. M. Rørvik, T. Lyngdal, R. Sæterli, A. T. J. van Helvoort, R. Holmestad, T. Grande and M.-A. Einarsrud, *Inorg. Chem.*, 2008, **47**, 3173-3181.
77. R. G. P. McQuaid, L. J. McGilly, P. Sharma, A. Gruverman and J. M. Gregg, *Nat Commun*, 2011, **2**, 404.
78. R. G. P. McQuaid, M. McMillen, L. W. Chang, A. Gruverman and J. M. Gregg, *J. Phys.: Condens. Matter*, 2012, **24**, 024204.
79. A. Schilling, R. M. Bowman, G. Catalan, J. F. Scott and J. M. Gregg, *Nano Lett.*, 2007, **7**, 3787-3791.
80. J. Q. Qi, Y. Wang, W. Ping Chen, L. Tu Li and H. Lai Wah Chan, *J. Solid State Chem.*, 2005, **178**, 279-284.
81. M. Niederberger, G. Garnweitner, N. Pinna and M. Antonietti, *J. Am. Chem. Soc.*, 2004, **126**, 9120-9126.
82. Y. Chen, W. Chen, F. Guo, M.-Y. Li, W. Liu and X.-Z. Zhao, *Chinese Physics B*, 2009, **18**, 3922.
83. J. A. Nelson and M. J. Wagner, *J. Am. Chem. Soc.*, 2002, **125**, 332-333.
84. S. Xu, B. J. Hansen and Z. L. Wang, *Nat Commun*, 2010, **1**, 93.
85. G. Xu, W. Jiang, M. Qian, X. Chen, Z. Li and G. Han, *Cryst Growth Des*, 2008, **9**, 13-16.
86. W. Lee, H. Han, A. Lotnyk, M. A. Schubert, S. Senz, M. Alexe, D. Hesse, S. Baik and U. Gosele, *Nat Nano*, 2008, **3**, 402-407.
87. S. Clemens and et al., *Nanotechnology*, 2009, **20**, 075305.
88. A. Bernal, A. Tselev, S. Kalinin and N. Bassiri-Gharb, *Adv. Mater.*, 2012, **24**, 1160-1165.
89. M. Alexe, C. Harnagea, D. Hesse and U. Gosele, *Appl. Phys. Lett.*, 1999, **75**, 1793-1795.
90. C.-K. Huang, Y.-H. Chen, Y.-C. Liang, T.-B. Wu, H.-L. Chen and W.-C. Chao, *Electrochem. Solid-State Lett.*, 2006, **9**, C51-C53.
91. Z. K. Shen, Z. H. Chen, H. Li, X. P. Qu, Y. Chen and R. Liu, *Appl. Surf. Sci.*, 2011, **257**, 8820-8823.
92. Z.-D. Li, Z.-K. Shen, W.-Y. Hui, Z.-J. Qiu, X.-P. Qu, Y.-F. Chen and R. Liu, *Microelectron. Eng.*, 2011, **88**, 2037-2040.
93. I. Szafraniak, C. Harnagea, R. Scholz, S. Bhattacharyya, D. Hesse and M. Alexe, *Appl. Phys. Lett.*, 2003, **83**, 2211-2213.
94. M.-W. Chu, I. Szafraniak, R. Scholz, C. Harnagea, D. Hesse, M. Alexe and U. Gosele, *Nat Mater*, 2004, **3**, 87-90.
95. M. Dawber, I. Szafraniak, M. Alexe and J. F. Scott, *J. Phys.: Condens. Matter*, 2003, **15**, L667.
96. I. Szafraniak, M. W. Chu, C. Harnagea, R. Scholz, D. Hesse and M. Alexe, *Integrated Ferroelectrics*, 2004, **61**, 231-238.
97. M. Torres, J. Ricote, L. Pardo and M. L. Calzada, *Integrated Ferroelectrics*, 2008, **99**, 95-104.
98. A. Roelofs, T. Schneller, K. Szot and R. Waser, *Appl. Phys. Lett.*, 2002, **81**, 5231-5233.
99. X. Y. Zhang, X. Zhao, C. W. Lai, J. Wang, X. G. Tang and J. Y. Dai, *Appl. Phys. Lett.*, 2004, **85**, 4190-4192.
100. Y. Kim, H. Han, Y. Kim, W. Lee, M. Alexe, S. Baik and J. K. Kim, *Nano Lett.*, 2010, **10**, 2141-2146.
101. J. F. Scott, H. J. Fan, S. Kawasaki, J. Banys, M. Ivanov, A. Krotkus, J. Macutkevic, R. Blinc, V. V. Laguta, P. Cevc, J. S. Liu and A. L. Kholkin, *Nano Lett.*, 2008, **8**, 4404-4409.
102. J. Kim, S. A. Yang, Y. C. Choi, J. K. Han, K. O. Jeong, Y. J. Yun, D. J. Kim, S. M. Yang, D. Yoon, H. Cheong, K. S. Chang, T. W. Noh and S. D. Bu, *Nano Lett.*, 2008, **8**, 1813-1818.
103. D. Pantel, S. Goetze, D. Hesse and M. Alexe, *ACS Nano*, 2011, **5**, 6032-6038.
104. B. A. Hernandez-Sanchez, K.-S. Chang, M. T. Scancella, J. L. Burris, S. Kohli, E. R. Fisher and P. K. Dorhout, *Chem. Mater.*, 2005, **17**, 5909-5919.
105. X. Chen, S. Xu, N. Yao and Y. Shi, *Nano Lett.*, 2010, **10**, 2133-2137.
106. X. Shiyou, S. Yong and K. Sang-Gook, *Nanotechnology*, 2006, **17**, 4497.
107. W. Wu, S. Bai, M. Yuan, Y. Qin, Z. L. Wang and T. Jing, *ACS Nano*, 2012.
108. L. J. McGilly and J. M. Gregg, *Nano Lett.*, 2011, **11**, 4490-4495.
109. V. Nagarajan, A. Stanishevsky and R. Ramesh, *Nanotechnology*, 2006, **17**, 338.
110. J. M. Marshall, S. Dunn and R. W. Whatmore, *Integrated Ferroelectrics*, 2004, **61**, 223-230.
111. R. Zhu, K. Zhu, J. Qiu, L. Bai and H. Ji, *Mater. Res. Bull.*, 2010, **45**, 969-973.
112. L. Hou, Y.-D. Hou, X.-M. Song, M.-K. Zhu, H. Wang and H. Yan, *Mater. Res. Bull.*, 2006, **41**, 1330-1336.
113. L. JingBing, W. Hao, H. YuDong, Z. ManKang, Y. Hui and Y. Masahiro, *Nanotechnology*, 2004, **15**, 777.
114. A. Anokhin, N. Lyanguzov, S. Roshal', Y. Yuzyuk and W. Wang, *Physics of the Solid State*, 2011, **53**, 1867-1871.
115. M. T. Buscaglia, M. Sennour, V. Buscaglia, C. Bottino, V. Kalyani and P. Nanni, *Cryst Growth Des*, 2011, **11**, 1394-1401.
116. H. Gu, Z. Hu, Y. Hu, Y. Yuan, J. You and W. Zou, *Colloids and Surfaces A: Physicochemical and Engineering Aspects*, 2008, **315**, 294-298.
117. D. Zhou, H. Gu, Y. Hu, Z. Qian, Z. Hu, K. Yang, Y. Zou, Z. Wang, Y. Wang, J. Guan and W. Chen, *J. Appl. Phys.*, 2010, **107**, 094105.
118. T. Minghua, S. Wei, Y. Feng, Z. Jun, D. Guangjun and H. Jianwei, *Nanotechnology*, 2009, **20**, 385602.
119. U. Shaislamov, J.-M. Yang and B. Yang, *Physica E: Low-dimensional Systems and Nanostructures*, 2012, **44**, 1649-1652.
120. R. Das, G. G. Khan and K. Mandal, *J. Appl. Phys.*, 2012, **111**, 104115-104116.
121. X. Y. Zhang, J. Y. Dai and C. W. Lai, *Prog. Solid State Chem.*, 2005, **33**, 147-151.

122. D. P. Dutta, O. D. Jayakumar, A. K. Tyagi, K. G. Girija, C. G. S. Pillai and G. Sharma, *Nanoscale*, 2010, **2**, 1149-1154.
123. L. Wang, A. Teleki, S. E. Pratsinis and P. I. Gouma, *Chem. Mater.*, 2008, **20**, 4794-4796.
124. H. Zhou, T.-J. Park and S. S. Wong, *J. Mater. Res.*, 2006, **21**, 2941-2947.
125. J. Varghese, C. O'Regan, N. Deepak, R. W. Whatmore and J. D. Holmes, *Chem. Mater.*, 2012, **24**, 3279-3284.
126. M. Nowak, P. Szperlich, Ł. Bober, J. Szala, G. Moskal and D. Stróż, *Ultrason. Sonochem.*, 2008, **15**, 709-716.
127. M. Nowak, B. Kauch, P. Szperlich, D. Stróz, J. Szala, T. Rzychon, L. Bober, B. Toron and A. Nowrot, *Ultrason. Sonochem.*, 2010, **17**, 487-493.
128. J. Varghese, S. Barth, L. Keeney, R. W. Whatmore and J. D. Holmes, *Nano Lett.*, 2012, **12**, 868-872.
129. M. J. Polking, J. J. Urban, D. J. Milliron, H. Zheng, E. Chan, M. A. Caldwell, S. Raoux, C. F. Kisielowski, J. W. Ager, R. Ramesh and A. P. Alivisatos, *Nano Lett.*, 2011, **11**, 1147-1152.
130. M. J. Polking, H. Zheng, R. Ramesh and A. P. Alivisatos, *J. Am. Chem. Soc.*, 2011, **133**, 2044-2047.
131. J. Y. Son, Y.-S. Shin, S.-W. Song, Y.-H. Shin and H. M. Jang, *The Journal of Physical Chemistry C*, 2011, **115**, 14077-14080.
132. Z. Hu, M. Tian, B. Nysten and A. M. Jonas, *Nat Mater*, 2009, **8**, 62-67.
133. Y. Liu, D. N. Weiss and J. Li, *ACS Nano*, 2009, **4**, 83-90.
134. C.-C. Hong, S.-Y. Huang, J. Shieh and S.-H. Chen, *Macromolecules*, 2012, **45**, 1580-1586.
135. S. J. Kang, I. Bae, Y. J. Shin, Y. J. Park, J. Huh, S.-M. Park, H.-C. Kim and C. Park, *Nano Lett.*, 2010, **11**, 138-144.
136. J. Martín, C. Mijangos, A. Sanz, T. A. Ezquerra and A. Nogales, *Macromolecules*, 2009, **42**, 5395-5401.
137. J. L. Lutkenhaus, K. McEnnis, A. Serghei and T. P. Russell, *Macromolecules*, 2010, **43**, 3844-3850.
138. B. A. Hernandez, K.-S. Chang, E. R. Fisher and P. K. Dorhout, *Chem. Mater.*, 2002, **14**, 480-482.
139. L. J. Guo, *Adv. Mater.*, 2007, **19**, 495-513.
140. J.-R. Fang, Z.-K. Shen, S. Yang, Q. Lu, J. Li, Y.-F. Chen and R. Liu, *Microelectron. Eng.*, 2011, **88**, 2033-2036.
141. K. Ishikawa, T. Nomura, N. Okada and K. Takada, *Jpn J Appl Phys 1*, 1996, **35**, 5196-5198.
142. K. Ishikawa, K. Yoshikawa and N. Okada, *Phys Rev B*, 1988, **37**, 5852-5855.
143. D. Mohanty, G. S. Chaubey, A. Yourdkhani, S. Adireddy, G. Caruntu and J. B. Wiley, *RSC Advances*, 2012, **2**, 1913-1916.
144. F. C. Meldrum and H. Cölfen, *Chem. Rev.*, 2008, **108**, 4332-4432.
145. Y. Li, F. Qian, J. Xiang and C. M. Lieber, *Mater. Today*, 2006, **9**, 18-27.
146. S. Barth, F. Hernandez-Ramirez, J. D. Holmes and A. Romano-Rodriguez, *Prog. Mater Sci.*, 2010, **55**, 563-627.
147. J.-P. Colinge, C.-W. Lee, A. Afzalian, N. D. Akhavan, R. Yan, I. Ferain, P. Razavi, B. O'Neill, A. Blake, M. White, A.-M. Kelleher, B. McCarthy and R. Murphy, *Nat Nano*, 2010, **5**, 225-229.
148. M. M. A. Hakim, M. Lombardini, K. Sun, F. Giustiniano, P. L. Roach, D. E. Davies, P. H. Howarth, M. R. R. de Planque, H. Morgan and P. Ashburn, *Nano Lett.*, 2012, **12**, 1868-1872.
149. X. Liu, Y.-Z. Long, L. Liao, X. Duan and Z. Fan, *ACS Nano*, 2012, **6**, 1888-1900.
150. Y. Xia, P. Yang, Y. Sun, Y. Wu, B. Mayers, B. Gates, Y. Yin, F. Kim and H. Yan, *Adv. Mater.*, 2003, **15**, 353-389.
151. J. T. Hu, T. W. Odom and C. M. Lieber, *Acc. Chem. Res.*, 1999, **32**, 435-445.
152. B. Weber, S. Mahapatra, H. Ryu, S. Lee, A. Fuhrer, T. C. G. Reusch, D. L. Thompson, W. C. T. Lee, G. Klimeck, L. C. L. Hollenberg and M. Y. Simmons, *Science*, 2012, **335**, 64-67.
153. S. J. Limmer, S. Seraji, M. J. Forbess, Y. Wu, T. P. Chou, C. Nguyen and G. Z. Cao, *Adv. Mater.*, 2001, **13**, 1269-1272.
154. S. B. Cho, M. Oledzka and R. E. Riman, *J. Cryst. Growth*, 2001, **226**, 313-326.
155. W. S. Yun, J. J. Urban, Q. Gu and H. Park, *Nano Lett.*, 2002, **2**, 447-450.
156. A. Magrez, E. Vasco, J. W. Seo, C. Dieker, N. Setter and L. Forró, *The Journal of Physical Chemistry B*, 2005, **110**, 58-61.
157. J. H. Jung, M. Lee, J.-I. Hong, Y. Ding, C.-Y. Chen, L.-J. Chou and Z. L. Wang, *ACS Nano*, 2011, **5**, 10041-10046.
158. Z. Shen, X. Qu, Y. Chen and R. Liu, *ACS Nano*, 2011, **5**, 6855-6860.
159. Z. Shen, Z. Chen, Q. Lu, Z. Qiu, A. Jiang, X. Qu, Y. Chen and R. Liu, *Nanoscale Research Letters*, 2011, **6**, 474.
160. S. Xu, G. Poirier and N. Yao, *Nano Lett.*, 2012, **12**, 2238-2242.
161. A. Rabenau, *Angewandte Chemie International Edition in English*, 1985, **24**, 1026-1040.
162. P. Szperlich, M. Nowak, L. Bober, J. Szala and D. Stroz, *Ultrason. Sonochem.*, 2009, **16**, 398-401.
163. A. Stanishevsky, S. Aggarwal, A. S. Prakash, J. Melngailis and R. Ramesh, *Journal of Vacuum Science & Technology B: Microelectronics and Nanometer Structures*, 1998, **16**, 3899-3902.
164. C. S. Ganpule, A. Stanishevsky, Q. Su, S. Aggarwal, J. Melngailis, E. Williams and R. Ramesh, *Appl. Phys. Lett.*, 1999, **75**, 409-411.
165. C. R. Martin, *Science*, 1994, **266**, 1961-1966.
166. D. Routkevitch, A. A. Tager, J. Haruyama, D. Almawlawi, M. Moskovits and J. M. Xu, *Ieee Transactions on Electron Devices*, 1996, **43**, 1646-1658.
167. C. Bae, H. Yoo, S. Kim, K. Lee, J. Kim, M. A. Sung and H. Shin, *Chem. Mater.*, 2008, **20**, 756-767.
168. K. Schwirn, W. Lee, R. Hillebrand, M. Steinhart, K. Nielsch and U. Gösele, *ACS Nano*, 2008, **2**, 302-310.
169. D. Yadlovker and S. Berger, *Phys Rev B*, 2005, **71**, 184112.
170. M. Alexe, D. Hesse, V. Schmidt, S. Senz, H. J. Fan, M. Zacharias and U. Gosele, *Appl. Phys. Lett.*, 2006, **89**, 172907.
171. J.-S. Lee, B.-I. Lee and S.-K. Joo, *Integrated Ferroelectrics*, 2000, **31**, 149-162.
172. T. D. Nguyen, J. M. Nagarah, Y. Qi, S. S. Nonnenmann, A. V. Morozov, S. Li, C. B. Arnold and M. C. McAlpine, *Nano Lett.*, 2010, **10**, 4595-4599.
173. R. D. Piner, J. Zhu, F. Xu, S. Hong and C. A. Mirkin, *Science*, 1999, **283**, 661-663.
174. J. Y. Son, Y.-H. Shin, S. Ryu, H. Kim and H. M. Jang, *J. Am. Chem. Soc.*, 2009, **131**, 14676-14678.
175. C. Harnagea, M. Alexe, J. Schilling, J. Choi, R. B. Wehrspohn, D. Hesse and U. Gosele, *Appl. Phys. Lett.*, 2003, **83**, 1827-1829.
176. M. Alexe and D. Hesse, *J Mater Sci*, 2006, **41**, 1-11.
177. J. C. Hulteen and R. P. Van Duyne, *Journal of Vacuum Science & Technology A: Vacuum, Surfaces, and Films*, 1995, **13**, 1553-1558.
178. W. Ma and D. Hesse, *Appl. Phys. Lett.*, 2004, **85**, 3214-3216.
179. M. Waegner, G. Suchaneck and G. Gerlach, *Integrated Ferroelectrics*, 2011, **123**, 75-80.
180. D. Byrne, A. Schilling, J. F. Scott and J. M. Gregg, *Nanotechnology*, 2008, **19**, 165608.
181. C. V. Cojocaru, C. Harnagea, A. Pignolet and F. Rosei, *IEEE Transactions on Nanotechnology*, 2006, **5**, 470-477.
182. H.-J. Shin, J. H. Choi, H. J. Yang, Y. D. Park, Y. Kuk and C.-J. Kang, *Appl. Phys. Lett.*, 2005, **87**, 113114.
183. X. Lu, Y. Kim, S. Goetze, X. Li, S. Dong, P. Werner, M. Alexe and D. Hesse, *Nano Lett.*, 2011, 3202–3206.
184. B. J. Rodriguez, X. S. Gao, L. F. Liu, W. Lee, Naumov, II, A. M. Bratkovsky, D. Hesse and M. Alexe, *Nano Lett.*, 2009, **9**, 1127-1131.
185. W. Lee, M. Alexe, K. Nielsch and U. Gösele, *Chem. Mater.*, 2005, **17**, 3325-3327.
186. Y. Kim, A. Kumar, A. Tselev, I. I. Kravchenko, H. Han, I. Vrejoiu, W. Lee, D. Hesse, M. Alexe, S. V. Kalinin and S. Jesse, *ACS Nano*, 2011, **5**, 9104-9112.
187. Y. Kim, A. Kumar, O. Ovchinnikov, S. Jesse, H. Han, D. Pantel, I. Vrejoiu, W. Lee, D. Hesse, M. Alexe and S. V. Kalinin, *ACS Nano*, 2011, **6**, 491-500.
188. H.-C. Kim, S.-M. Park and W. D. Hinsberg, *Chem. Rev.*, 2009, **110**, 146-177.
189. J. K. Kim, S. Y. Yang, Y. Lee and Y. Kim, *Prog. Polym. Sci.*, 2010, **35**, 1325-1349.
190. I. W. Hamley, *Nanotechnology*, 2003, **14**, R39.
191. D. J. C. Herr, *J. Mater. Res.*, 2011, **26**, 122-139.
192. S.-M. Park, X. Liang, B. D. Harteneck, T. E. Pick, N. Hiroshiba, Y. Wu, B. A. Helms and D. L. Olynick, *ACS Nano*, 2011, **5**, 8523-8531.

This journal is © The Royal Society of Chemistry [year]

193. J. W. Jeong, W. I. Park, L.-M. Do, J.-H. Park, T.-H. Kim, G. Chae and Y. S. Jung, *Advanced Materials*, 2012, n/a-n/a.
194. E. Akcoltekin, T. Peters, R. Meyer, A. Duvenbeck, M. Klusmann, I. Monnet, H. Lebius and M. Schleberger, *Nat Nano*, 2007, **2**, 290-294.
195. Z. L. Wang, *Adv. Mater.*, 2012, Early view, http://dx.doi.org/10.1002/adma.201104365.
196. Z. L. Wang, *Adv. Mater.*, 2012, **24**, 280-285.
197. Z. L. Wang and J. Song, *Science*, 2006, **312**, 242-246.
198. J. F. Scott, *Ferroelectrics*, 2005, **314**, 207-222.
199. Y. Lin, Y. Liu and H. A. Sodano, *Appl. Phys. Lett.*, 2009, **95**, 122901-122903.
200. B. Im, H. Jun, K. H. Lee, S.-H. Lee, I. K. Yang, Y. H. Jeong and J. S. Lee, *Chem. Mater.*, 2010, **22**, 4806-4813.
201. J. Hwichan, I. Badro, L. Kyung Hee, Y. Il Kyu, J. Yoon Hee and L. Jae Sung, *Nanotechnology*, 2012, **23**, 135602.
202. Y.-Z. Chen, T.-H. Liu, C.-Y. Chen, C.-H. Liu, S.-Y. Chen, W.-W. Wu, Z. L. Wang, J.-H. He, Y.-H. Chu and Y.-L. Chueh, *ACS Nano*, 2012, **6**, 2826-2832.
203. B. Im, H. Jun, K. H. Lee and J. S. Lee, *CrystEngComm*, 2011, **13**, 7212-7215.
204. S. V. Kalinin and et al., *Rep. Prog. Phys.*, 2010, **73**, 056502.
205. A. Gruverman and S. V. Kalinin, in *Frontiers of Ferroelectricity*, 2007, pp. 107-116.
206. L. Bocher, A. Gloter, A. Crassous, V. Garcia, K. March, A. Zobelli, S. Valencia, S. Enouz-Vedrenne, X. Moya, N. D. Marthur, C. Deranlot, S. Fusil, K. Bouzehouane, M. Bibes, A. Barthélémy, C. Colliex and O. Stéphan, *Nano Lett.*, 2011, **12**, 376-382.
207. C.-L. Jia, S.-B. Mi, K. Urban, I. Vrejoiu, M. Alexe and D. Hesse, *Nat Mater*, 2008, **7**, 57-61.
208. C. T. Nelson, P. Gao, J. R. Jokisaari, C. Heikes, C. Adamo, A. Melville, S.-H. Baek, C. M. Folkman, B. Winchester, Y. Gu, Y. Liu, K. Zhang, E. Wang, J. Li, L.-Q. Chen, C.-B. Eom, D. G. Schlom and X. Pan, *Science*, 2011, **334**, 968-971.
209. A. Schilling, D. Byrne, G. Catalan, K. G. Webber, Y. A. Genenko, G. S. Wu, J. F. Scott and J. M. Gregg, *Nano Lett.*, 2009, **9**, 3359-3364.
210. S. Jesse, A. P. Baddorf and S. V. Kalinin, *Appl. Phys. Lett.*, 2006, **88**, 062908.
211. S. Dunn, D. Cullen, E. Abad-Garcia, C. Bertoni, R. Carter, D. Howorth and R. W. Whatmore, *Appl. Phys. Lett.*, 2004, **85**, 3537-3539.
212. S. Dunn, C. P. Shaw, Z. Huang and R. W. Whatmore, *Nanotechnology*, 2002, **13**, 456.
213. S. Dunn and R. W. Whatmore, *J. Eur. Ceram. Soc.*, 2002, **22**, 825-833.
214. S. Dunn, Q. Zhang and R. W. Whatmore, *Integrated Ferroelectrics*, 2002, **46**, 87-94.
215. B. J. Rodriguez, S. Jesse, M. Alexe and S. V. Kalinin, *Adv. Mater.*, 2008, **20**, 109-114.
216. Y. Ivry, D. Chu and C. Durkan, *Appl. Phys. Lett.*, 2009, **94**, 162903.
217. M. J. Polking, M.-G. Han, A. Yourdkhani, V. Petkov, C. F. Kisielowski, V. V. Volkov, Y. Zhu, G. Caruntu, A. P. Alivisatos and R. Ramesh, *Nature Materials*, 2012, **11**, 700-709.
218. Y. Shiratori, C. Pithan, J. Dornseiffer and R. Waser, *Journal of Raman Spectroscopy*, 2007, **38**, 1300-1306.
219. Y. Shiratori, C. Pithan, J. Dornseiffer and R. Waser, *Journal of Raman Spectroscopy*, 2007, **38**, 1288-1299.
220. D. A. Tenne, P. Turner, J. D. Schmidt, M. Biegalski, Y. L. Li, L. Q. Chen, A. Soukiassian, S. Trolier-McKinstry, D. G. Schlom, X. X. Xi, D. D. Fong, P. H. Fuoss, J. A. Eastman, G. B. Stephenson, C. Thompson and S. K. Streiffer, *Phys. Rev. Lett.*, 2009, **103**, 177601.
221. D. A. Tenne, A. Bruchhausen, N. D. Lanzillotti-Kimura, A. Fainstein, R. S. Katiyar, A. Cantarero, A. Soukiassian, V. Vaithyanathan, J. H. Haeni, W. Tian, D. G. Schlom, K. J. Choi, D. M. Kim, C. B. Eom, H. P. Sun, X. Q. Pan, Y. L. Li, L. Q. Chen, Q. X. Jia, S. M. Nakhmanson, K. M. Rabe and X. X. Xi, *Science*, 2006, **313**, 1614-1616.
222. R. Kretschmer and K. Binder, *Phys Rev B*, 1979, **20**, 1065-1076.
223. M. Alexe, C. Harnagea, A. Visinoiu, A. Pignolet, D. Hesse and U. Gosele, *Scripta Mater.*, 2001, **44**, 1175-1179.
224. M. Dawber, P. Chandra, P. B. Littlewood and J. F. Scott, *J. Phys.: Condens. Matter*, 2003, **15**, L393.
225. T. M. Shaw, S. Trolier-McKinstry and P. C. McIntyre, *Annu. Rev. Mater. Sci.*, 2000, **30**, 263-298.
226. T. Tybell, C. H. Ahn and J. M. Triscone, *Appl. Phys. Lett.*, 1999, **75**, 856-858.
227. B. Jiang, J. L. Peng, L. A. Bursill and W. L. Zhong, *J. Appl. Phys.*, 2000, **87**, 3462-3467.
228. S. Kohiki, S. Takada, A. Shimizu, K. Yamada, H. Higashijima and M. Mitome, *J. Appl. Phys.*, 2000, **87**, 474-478.
229. J. Junquera and P. Ghosez, *Nature*, 2003, **422**, 506-509.
230. W. L. Zhong, Y. G. Wang, P. L. Zhang and B. D. Qu, *Phys Rev B*, 1994, **50**, 698-703.
231. Y. G. Wang, W. L. Zhong and P. L. Zhang, *Phys Rev B*, 1995, **51**, 17235-17238.
232. Y. G. Wang, W. L. Zhong and P. L. Zhang, *Solid State Commun.*, 1994, **92**, 519-523.
233. W. Sun, *J. Appl. Phys.*, 2006, **100**, 083503-083507.
234. S. A. Basun, G. Cook, V. Y. Reshetnyak, A. V. Glushchenko and D. R. Evans, *Phys Rev B*, 2011, **84**, 024105.
235. T. Hoshina, H. Kakemoto, T. Tsurumi, S. Wada and M. Yashima, *J. Appl. Phys.*, 2006, **99**, 054311-054318.
236. L. Huang, Z. Jia, I. Kymissis and S. O'Brien, *Adv. Funct. Mater.*, 2010, **20**, 554-560.
237. S. Singh, *Advanced Science Letters*, 2012, **11**, 39-42.
238. M. B. Smith, K. Page, T. Siegrist, P. L. Redmond, E. C. Walter, R. Seshadri, L. E. Brus and M. L. Steigerwald, *J. Am. Chem. Soc.*, 2008, **130**, 6955-6963.
239. J. Y. Son and I. Jung, *J. Am. Ceram. Soc.*, 2012, **95**, 480-482.
240. G. Suyal, E. Colla, R. Gysel, M. Cantoni and N. Setter, *Nano Lett.*, 2004, **4**, 1339-1342.
241. I. I. Naumov and H. Fu, *Phys. Rev. Lett.*, 2005, **95**, 247602.
242. J. E. Spanier, A. M. Kolpak, J. J. Urban, I. Grinberg, L. Ouyang, W. S. Yun, A. M. Rappe and H. Park, *Nano Lett.*, 2006, **6**, 735-739.
243. K. Rabe, M. Dawber, C. Lichtensteiger, C. Ahn and J.-M. Triscone, in *Physics of Ferroelectrics: A Modern Perspective*, Springer Berlin / Heidelberg, 2007, vol. 105, pp. 1-30.
244. C. W. Beier, M. A. Cuevas and R. L. Brutchey, *Langmuir*, 2009, **26**, 5067-5071.
245. D. Li, M. H. Zhao, J. Garra, A. M. Kolpak, A. M. Rappe, D. A. Bonnell and J. M. Vohs, *Nat Mater*, 2008, **7**, 473-477.
246. L. Louis, P. Gemeiner, I. Ponomareva, L. Bellaiche, G. Geneste, W. Ma, N. Setter and B. Dkhil, *Nano Lett.*, 2010, **10**, 1177-1183.
247. R. Yasinov, M. Nitzani and S. Berger, *Ferroelectrics*, 2009, **390**, 153 - 159.
248. Y. Qi, J. Kim, T. D. Nguyen, B. Lisko, P. K. Purohit and M. C. McAlpine, *Nano Lett.*, 2011, **11**, 1331-1336.
249. M. E. Lines and A. M. Glass, in *Principles and Applications of Ferroelectrics and Related Materials*, Oxford University Press, Oxford, 1977, pp. 559-607.
250. N. Setter, D. Damjanovic, L. Eng, G. Fox, S. Gevorgian, S. Hong, A. Kingon, H. Kohlstedt, N. Y. Park, G. B. Stephenson, I. Stolitchnov, A. K. Taganstev, D. V. Taylor, T. Yamada and S. Streiffer, *J. Appl. Phys.*, 2006, **100**, 051606-051646.
251. D. Hadnagy, in *The Industrial Physicist*, American Institute of Physics, 1999, vol. 5, pp. 26-28.
252. R. W. Whatmore, *Ferroelectrics*, 1991, **118**, 241-259.
253. J. Fang, H. Frederich and L. Pilon, *J. Heat Transfer*, 2010, **132**, 092701.
254. S. B. Lang, *Phys. Today*, 2005, **58**, 31-36.
255. J. F. Scott, *Integrated Ferroelectrics*, 2000, **31**, 139-147.
256. A. Chanthbouala, A. Crassous, V. Garcia, K. Bouzehouane, S. Fusil, X. Moya, J. Allibe, B. Dlubak, J. Grollier, S. Xavier, C. Deranlot, A. Moshar, R. Proksch, N. D. Mathur, M. Bibes and A. Barthelemy, *Nat Nano*, 2012, **7**, 101-104.
257. S. Das and J. Appenzeller, *Nano Lett.*, 2011, **11**, 4003-4007.
258. D. Y. Kusuma, C. A. Nguyen and P. S. Lee, *The Journal of Physical Chemistry B*, 2010, **114**, 13289-13293.
259. J. Hoffman, X. Pan, J. W. Reiner, F. J. Walker, J. P. Han, C. H. Ahn and T. P. Ma, *Adv. Mater.*, 2010, **22**, 2957-2961.
260. D. Lee, S. M. Yang, T. H. Kim, B. C. Jeon, Y. S. Kim, J.-G. Yoon, H. N. Lee, S. H. Baek, C. B. Eom and T. W. Noh, *Adv. Mater.*, 2012, **24**, 402-406.

261. D. I. Bilc, F. D. Novaes, J. Íñiguez, P. Ordejón and P. Ghosez, *ACS Nano*, 2012, **6**, 1473-1478.
262. P. Maksymovych, A. N. Morozovska, P. Yu, E. A. Eliseev, Y.-H. Chu, R. Ramesh, A. P. Baddorf and S. V. Kalinin, *Nano Lett.*, 2011, **12**, 209-213.
263. H. Ko, K. Ryu, H. Park, C. Park, D. Jeon, Y. K. Kim, J. Jung, D.-K. Min, Y. Kim, H. N. Lee, Y. Park, H. Shin and S. Hong, *Nano Lett.*, 2011, **11**, 1428-1433.
264. A. Gruverman, D. Wu, H. Lu, Y. Wang, H. W. Jang, C. M. Folkman, M. Y. Zhuravlev, D. Felker, M. Rzchowski, C. B. Eom and E. Y. Tsymbal, *Nano Lett.*, 2009, **9**, 3539-3543.
265. Y. Hu, L. Lin, Y. Zhang and Z. L. Wang, *Adv. Mater.*, 2012, **24**, 110-114.
266. Y. Qi, N. T. Jafferis, K. Lyons, C. M. Lee, H. Ahmad and M. C. McAlpine, *Nano Lett.*, 2010, **10**, 524-528.
267. S. Cha, S. M. Kim, H. Kim, J. Ku, J. I. Sohn, Y. J. Park, B. G. Song, M. H. Jung, E. K. Lee, B. L. Choi, J. J. Park, Z. L. Wang, J. M. Kim and K. Kim, *Nano Lett.*, 2011, **11**, 5142-5147.
268. A. N. Morozovska, E. A. Eliseev, G. S. Svechnikov and S. V. Kalinin, *J. Appl. Phys.*, 2010, **108**, 042009.
269. T. Zhou, J.-W. Zha, R.-Y. Cui, B.-H. Fan, J.-K. Yuan and Z.-M. Dang, *ACS Applied Materials & Interfaces*, 2011, **3**, 2184-2188.
270. K. Garrity, A. M. Kolpak, S. Ismail-Beigi and E. I. Altman, *Adv. Mater.*, 2010, **22**, 2969-2973.
271. M. N. Almadhoun, U. S. Bhansali and H. N. Alshareef, *J. Mater. Chem.*, 2012, **22**, 11196-11200.
272. P. Kim, N. M. Doss, J. P. Tillotson, P. J. Hotchkiss, M.-J. Pan, S. R. Marder, J. Li, J. P. Calame and J. W. Perry, *ACS Nano*, 2009, **3**, 2581-2592.
273. J. Li, J. Claude, L. E. Norena-Franco, S. I. Seok and Q. Wang, *Chem. Mater.*, 2008, **20**, 6304-6306.
274. K.-I. Park, M. Lee, Y. Liu, S. Moon, G.-T. Hwang, G. Zhu, J. E. Kim, S. O. Kim, D. K. Kim, Z. L. Wang and K. J. Lee, *Adv. Mater.*, 2012, **24**, 2999-3004.
275. A. Tavakkoli K. G., K. W. Gotrik, A. F. Hannon, A. Alexander-Katz, C. A. Ross and K. K. Berggren, *Science*, 2012, **336**, 1294-1298.

This journal is © The Royal Society of Chemistry [year]

5
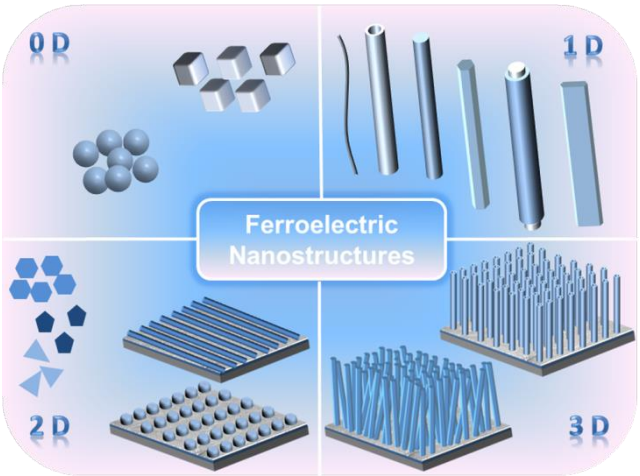
Table of contents Graphics